ARTICLE IN PRESS
JID: JMAA [m5+;September 30, 2020;23:2]

Available online at www.sciencedirect.com

ScienceDirect

Journal of Magnesium and Alloys xxx (xxxx) xxx

www.elsevier.com/locate/jma

Full Length Article

Investigating TiO_2–HA–PCL hybrid coating as an efficient corrosion resistant barrier of ZM21 Mg alloy ☆

Navdeep Singh[a], Uma Batra[a], Kamal Kumar[b,*], Anil Mahapatro[c]

[a] Department of Metallurgical and Materials Engineering, Punjab Engineering College, Chandigarh 160012, India
[b] Department of Mechanical Engineering, Punjab Engineering College, Chandigarh 160012, India
[c] Department of Biomedical Engineering, Wichita State University, Wichita, KS 67260, United States

Received 12 April 2020; received in revised form 25 June 2020; accepted 1 August 2020
Available online xxx

Abstract

Surface modification for improving corrosion resistance of Mg alloys is highly demanded for degradable orthopedic and cardiovascular devices. The research reports the design and development of TiO_2–HA composite and novel TiO_2–HA–PCL hybrid coating belonging to the unique class of inorganic organic hybrid with striking features that are explored for the first time in the corrosion resistance of Mg alloys. Sol–gel dip coating combined with non-solvent induced phase separation is used to create the hybrid coating. TiO_2–HA–PCL hybrid coating introduces strong hydrogen bonding between TiO_2–HA inorganic matrix and PCL organic layer in addition to the Vander wall electrostatic interaction of the later with the Mg substrate which in turn enhance adhesion strength to about 1.5 times of TiO_2–HA coating. The corrosion potentials for TiO_2–HA–PCL and TiO_2–HA were found to be −0.407 V and −1.017 V (vs Ag/AgCl), respectively. The current densities of TiO_2–HA–PCL and TiO_2–HA were found to be 7.31×10^{-8} A/cm^2 and 4.03×10^{-4} A/cm^2 respectively. The corrosion resistance of coatings was confirmed by immersion testing by weight loss, pH changes and H_2 evolution measurements at interval of 7 days till 28 days. The present TiO_2–HA–PCL coating in comparison to TiO_2–HA coating demonstrate nearly 6% less weight loss. The outcome of the present work was compared with the similar coatings in recent past. The work done ingresses enhancing the corrosion resistance of Mg alloys, which fulfill the dreams of future degradable orthopedic and cardiovascular devices.

Keywords: Corrosion resistance; TiO_2–HA–PCL; Contact angle; Adhesion strength.

1. Introduction

Worldwide research on orthopedic devices using degradable biomaterials such as magnesium (Mg) alloys has been accelerated in recent past. The intent is to reduce the need of second surgery for implant removal after complete healing of tissues and the severe stress shielding of permanent implants [1]. Due to limitations of permanent implant materials, it is necessary to find alternative degradable implant materials. Mg can be a promising and fascinating alternative biomaterial because of its Young's modulus (45 GPa) similar to that of human bone (40–57Gpa), light weight (density = 1.74 g/cm^3) and biodegradability in a physiological environment. Mg participates in essential metabolic processes

☆ **Statement of novelty:** Mg and its alloys are not developed fully as orthopedic implant element due to high degradation rate in physiological media. A TiO_2–HA–PCL hybrid coating is produced on ZM21 Mg alloy that reduced the Ecorr from −1.444 V (Ag/AgCl) for machined ZM21 Mg sample to −0.407 V (Ag/AgCl). The microporous layer on top facilitates the passage of H_2 gas, as a result no delamination is reported for the period of 28 days of immersion in SBF. Electrostatic interaction of PCL with Mg of substrate and its hydrogen bonding with HA of TiO_2–HA layer provide good adhesion strength well sustained during 28 days of immersion test. A compact corrosion product developed over TiO_2–HA–PCL coating indicating its better bioactivity, faster bone growth tendency and corrosion resistance.

* Corresponding author.
E-mail addresses: kamaljangra84@gmail.com, kamaljangra@pec.edu.in (K. Kumar).

https://doi.org/10.1016/j.jma.2020.08.003

like mitochondrial activity, nucleic acid synthesis and other cellular functions in human body [2]. The excessive amount of Mg is excreted from body as waste product [3]. Recently, different compositions of Mg alloys and coatings have been explored to improve degradation resistance by researchers but the rapid degradation of Mg alloys in physiological environment is still a challenge for the orthopedic application [4–6]. The strategic idea in this research field is to delay initial rapid corrosion and control of its degradation. The key point is retardation of corrosion process and not its complete stoppage [7].

Many recent studies have focused on the application of coatings on Mg surface and have found that the non-biodegradable coatings pose two most serious problems: (i) its remains in the human body may lead to undesirable effects like inflammation etc., (ii) localized corrosion due to the presence of cracks, discontinuities in the coating [6]. This raises considerable interest in the biodegradable and bioactive coatings to combat the above problems.

In terms of the bioactivity, Hydroxyapatite (HA) coating has been recommended in past due to its comparable chemical composition and crystallographic structure to the mineral component of natural bone [8]. But poor adhesion strength, brittleness and fragile nature of HA coatings demands its use in combination with other materials for load bearing application. So far, HA has been used as reinforcement in bio-inert ceramics like TiO_2 or ZrO_2 matrix to produce composite coatings that resulted in chemical stability compared to apatite structure [9]. HA reinforced TiO_2 coating has displayed good bioactivity and faster bone growth as well as corrosion resistance. Moreover, TiO_2–HA coating has higher bonding strength than HA coating [10]. Cell culture studies have reported improved biocompatibility and cell adhesion on HA–TiO_2 coated alloy [11]. While HA–TiO_2 coating on Mg alloy is porous and has low adhesion strength, this promotes penetration of electrolyte leading to decreased protection and compromised mechanical properties [12–14]. Biodegradable and biocompatible polymers such as polyacrylic acid (PAA), polycaprolactone (PCL), polylactic acid (PLA) and poly(lactic-co glycolic) acid (PLGA) degrade slowly, by water uptake and hydrolysis, releasing biocompatible by-products that are either used in various metabolic processes or excreted from the body [15]. While these polymers have been efficient to control the degradation rate and to functionalize the surface of Mg implants [16,17], the dissolution of the polymer and its hydrolysis leads to local pH acidification that further accelerates corrosion of Mg [18]. Among the mentioned polymers, PCL is inexpensive and is a fully degradable [19]. PCL is a U.S. Food and Drug Administration approved implantable material. PCL coatings have remarkable toughness and good biocompatibility [20,21]. PCL has an intrinsic hydrophobic chemical nature, and its poor surface wetting and interaction with biological fluids avoid cell adhesion and proliferation. It is a semi-crystalline aliphatic polymer that displayed slower degradation rate and higher fracture energy than most biocompatible polymers [22–25].

Based on these characteristics, PCL has been investigated for various biomedical applications [26]. Wong et al. has reported that PCL coating on AZ 91 Mg alloy resulted in good biocompatibility but it showed poor bioactivity and poor adhesion strength [27]. From the literature, it is obvious that a singular coating has not been able to fulfill requirements for the development of a bio-implant comprehensively. So far, various composite and hybrid coating strategies have been adopted by researchers. For example, Bakhsheshi-rad et al. applied hybrid coating comprising Fluorine doped HA–PCL on Mg-2Zn-3Ce alloy thereby resulting in the shift of E_{corr} from −1.60 to −1.25 V [28]. Chen et al. prepared PDA-TiO_2 hybrid coating on pure Mg and the E_{corr} improved from −1.58 V for pure Mg to −1.28 V [29]. Abdalla-hey et al. fabricated nHAp-PCL composite coating on AM50 Mg alloy and E_{corr} improved from −1.340 to −1.21 V for coated substrate [30]. The corrosion potential (E_{corr}) for various other hybrid coatings reported for Mg alloy has E_{corr} ranging from −1.728 to −1.057 V [31]. However, no study has been carried out on TiO_2–HA–PCL hybrid coatings as biodegradable and bioactive coatings on Mg-base substrate. In addition, the relationship between physicochemical properties of TiO_2–HA–PCL hybrid coating and Mg substrate corrosion are still unclear. Thus the research is still required to define an appropriate hybrid coating that is biodegradable, bioactive and suits the application requirement.

In the present study, the effect of hybrid coating comprising TiO_2–HA (inorganic part) and PCL (organic part) on its coating properties, electrochemical corrosion and degradation of Mg-base substrate were examined.

Wire electric discharge machining (WEDM) was employed for machining of Mg-base substrates. WEDM is a non-contact machining suitable for conductive metallic materials irrespective of their hardness that provides high dimensional accuracy and complex geometries required for the manufacturing of bio-implants. Manufacturing processes directly affect the surface and sub-surface properties of the implants and hence affect the corrosion, bio-functionality and fatigue life [32,33].

The hybrid coating was fabricated on ZM21 alloy using a facile wet chemical method in order to obtain uniformly distributed interconnected pores in PCL layers which would be beneficial in two ways. The proposed hybrid coating aims to slow down the degradation of Mg substrate rather complete stoppage as done by polymer coatings. Additionally, the chances of localized degradation would be reduced, often encountered in the inorganic coatings. For this purpose, TiO_2 and HA were selected as promising inorganic components which are bioactive and PCL was chosen as organic component which is biodegradable. Dip coating of hybrid coating on ZM21 were characterized by a number of techniques. The corrosion behavior of ZM21 substrate and coated samples was measured by Potential Polarization curves, EIS and immersion testing in simulated body fluid. The results of this research are optimistic with the promising use of developed hybrid coating in the field of orthopedic devices production.

Please cite this article as: N. Singh, U. Batra, K. Kumar et al., Investigating TiO2–HA–PCL hybrid coating as an efficient corrosion resistant barrier of ZM21 Mg alloy, Journal of Magnesium and Alloys, https://doi.org/10.1016/j.jma.2020.08.003

Table 1
WEDM parameters for machining of ZM21 Mg alloy.

WEDM Parameter	Pulse on time(μs)	Pulse off time(μs)	Peak current (amp)	Wire feed rate (m/min)	Servo feed (rpm)	Servo voltage (V)
Value	103	52	12	2	2100	20

2. Experimental

2.1. Materials and substrate preparation

A 7 mm thick extruded plate of ZM21 Mg alloy with a nominal composition of Mg–2.0Zn–1.0Mn (wt%) was machined into 20 × 20 × 4 mm samples using wire electric discharge machining WEDM (ELPULS 15 Electronica, India) at given parameters (Table 1). The machined samples were polished down to 1200 grit on SiC paper wet with ethanol and then ultrasonically cleaned. As-polished substrates were used to deposit the coatings.

2.2. Preparation of coatings

2.2.1. TiO_2–HA coating

The TiO_2 sol was prepared by dropwise adding titanium(IV) n-butoxide (TiO_2, Alfa-Aesar, USA) to a mixture of ethanol (EtOH) and acetic acid (HAc) using the molar ratio of TiO_2:EthOH:HAc::9:1:0.1 while continuous stirring at 600 rpm at 45 °C for 1 h. The acetic acid acts as a chelating agent and retards hydrolysis of titanium alkoxide [34]. Nanocrystalline pure hydroxyapatite powder was synthesized by methodology given by Batra et al. [35]. The nanopowder synthesized by sol–gel route was mixed with TiO_2 Sol (1:1 w/v) and stirred continuously for 24 h to obtain homogenous TiO_2–HA sol as shown in Fig. 1. In the present work, TiO_2–HA composite coating was deposited onto the polished ZM21 Mg alloy substrate by dip-coating at withdrawal speed of 5 mm/min with 1 min immersion time. The dip coating cycle was repeated for five times and each cycle was followed by drying at 60 °C for 1 h. The coated samples were calcined at 350 °C for 3 h according to experimentally determined conditions in order to transform amorphous TiO_2 to anatase phase and retain the HA phase as such. The anatase phase is more stable and biocompatible than rutile phase [36].

2.2.2. TiO_2–HA–PCL coating

The TiO_2−HA–PCL hybrid coating was deposited onto the TiO_2–HA coated samples by dip-coating. A chloroform solution of PCL prepared with 5% (w/v) prepared by dissolving PCL pellets (M_n= 80,000, Sigma-Aldrich) in Trichloromethane (TCL) while continuous stirring at 500 rpm for 3 h. The dip coating is performed at a withdrawal speed of 10 mm/min with immersion time of 1 min. The dip coating cycle was repeated for five cycles and each cycle was followed by drying at 30 °C for 1 h. The coated samples were heat treated at 50 °C for 12 h for uniform densification of polymeric coating. An interconnected microporous layer of PCL layer was fabricated onto the TiO_2–HA–PCL coated sample from the previous step by using non-solvent induced phase separation (NIPS) technique [37–39]. The schematic representation of coating process is shown in Fig. 2.

2.3. Surface morphology and adhesion strength

A JSM-IT100 scanning electron microscope (SEM) with energy dispersive spectrometer (EDS) was employed to characterize the morphology and elemental composition of as-machined surface, as-polished substrate, TiO_2–HA coated surface, and TiO_2–HA–PCL coated surface. The cross-section of coated samples was examined using SEM to measure the thickness of coatings. The surfaces after electrochemical corrosion and degradation studies were also observed using SEM-EDS. Fourier transform infrared spectroscopy (FT-IR, Bruker OPTIK) was used in the spectral domain of 400–4000 cm^{-1} at a resolution of 2 cm^{-1}. X-ray diffraction (XRD) was performed by Cu-Kα radiation over diffraction angles of 10° to 99° to detect the phases and crystalline structures of coatings using X'PERT Pro-Panalytical XRD. The crystallite sizes of TiO_2, HA powders were also calculated by XRD using Scherrer equation $D = k\lambda/\beta\cos\theta$ where, $k = 0.94$, $\lambda = 1.54178$ Å, β is full width at half maximum (FWHM) and θ is Bragg's law diffraction angle [40]. Contact angles (CA) measurements were carried out with simulated body fluid (SBF) by using Drop Shape Analyzer (DSA25S KRÚSS GmbH, Germany to determine hydrophobicity and surface properties of substrate and coatings. In the present work, 10μl SBF drop was used. The adhesion strength of TiO_2–HA and TiO_2-HA–PCL coatings applied on as-polished substrates was measured using scratch tester (TR-104, Ducom, USA). The scratch test was performed at a scratch speed of 10 mm/min over a scratch length of 3 mm according to ASTM standard C 1624-05. Three samples were tested for each type of coating and an average value of load has been reported. Cross-cut tape adhesion test was performed on PCL coated, TiO_2–HA coated and TiO_2–HA–PCL hybrid coated ZM21 Mg alloy according to ASTM standard D3359-17.

2.4. Electrochemical corrosion study and immersion test

All the electrochemical measurements were carried out using an electrochemical workstation (Autolab PGSTAT-302N, Metrohm, Switzerland) with three electrode configuration: Ag/AgCl (1 M KCL) and graphite rod served as reference electrode and counter electrode respectively, the samples (surface area of 1 cm^2) was the working electrode and the electrolyte was SBF at 37 °C. The SBF was prepared according to Kokubo et al. and it was buffered at pH 7.4 with tris-hydroxymethyl aminomethane and 0.1 M HCl [41]. The ion

Please cite this article as: N. Singh, U. Batra, K. Kumar et al., Investigating TiO2–HA–PCL hybrid coating as an efficient corrosion resistant barrier of ZM21 Mg alloy, Journal of Magnesium and Alloys, https://doi.org/10.1016/j.jma.2020.08.003

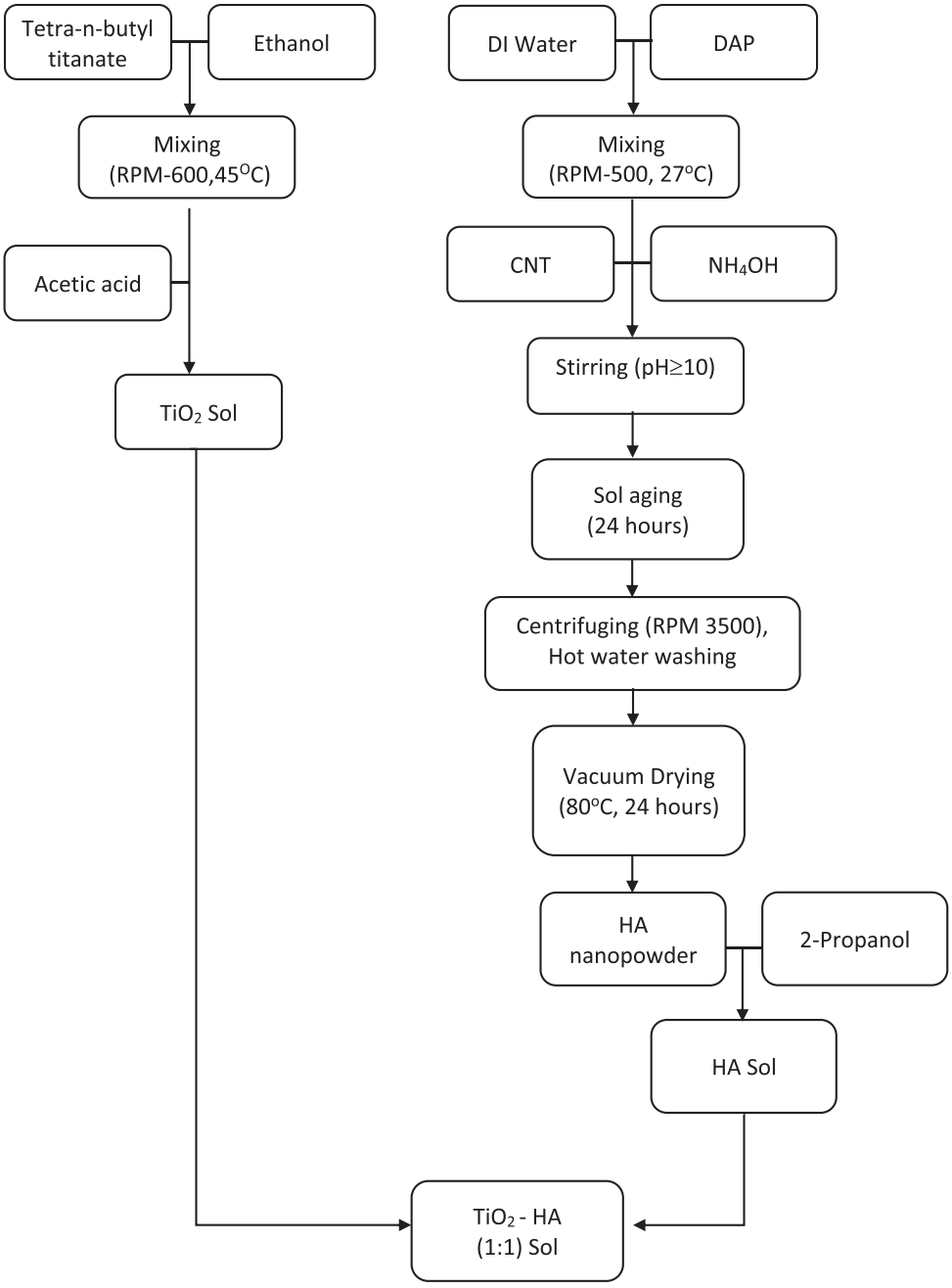

Fig. 1. Flowchart for the preparation TiO_2–HA composite sol.

concentrations in the SBF solution was 142.0 Na^+, 5.0 K^+, 1.5 Mg^{2+}, 2.5 Ca^{2+}, 147.8 Cl^-, 4.2 HCO^{3-}, 1.0 HPO^{4-}, and 0.5 SO_4^{2-} mM, being close to those in human blood plasma [42]. Potentiodynamic polarization (PDP) were performed at a 1 mVs^{-1} scan rate using potential window −900 mV to +1400 mV at step potential of 1 mV. Electrochemical Impedance Spectroscopy (EIS) was performed using same electrochemical workstation (Autolab instrument) Nova version 1.10. Nyquist plots were obtained for as-machined, as-polished, TiO_2–HA coated, TiO_2–HA–PCL coated samples at pre-determined OCP values of −1.473 V, −1.447 V, −1.112 V, −0.261 V respectively (vs Ag/AgCl) in the frequency range of 0.01 Hz to 100kH and 10 mV of amplitude.

In order to further investigate the degradation behavior, the immersion test was performed on the as-machined, as-polished, TiO_2–HA coated, TiO_2–HA–PCL coated samples according to ASTM G31-72. For the present work, the samples were immersed in SBF at 37± 1 °C for 7d, 14d, 21d and 28d and the volume to exposure area ratio was kept same as 0.20 ml/mm^2. The corroded samples were cleaned with chromic acid and subsequently rinsed with deionized water and dried in vacuum oven. The weight loss

Please cite this article as: N. Singh, U. Batra, K. Kumar et al., Investigating TiO2–HA–PCL hybrid coating as an efficient corrosion resistant barrier of ZM21 Mg alloy, Journal of Magnesium and Alloys, https://doi.org/10.1016/j.jma.2020.08.003

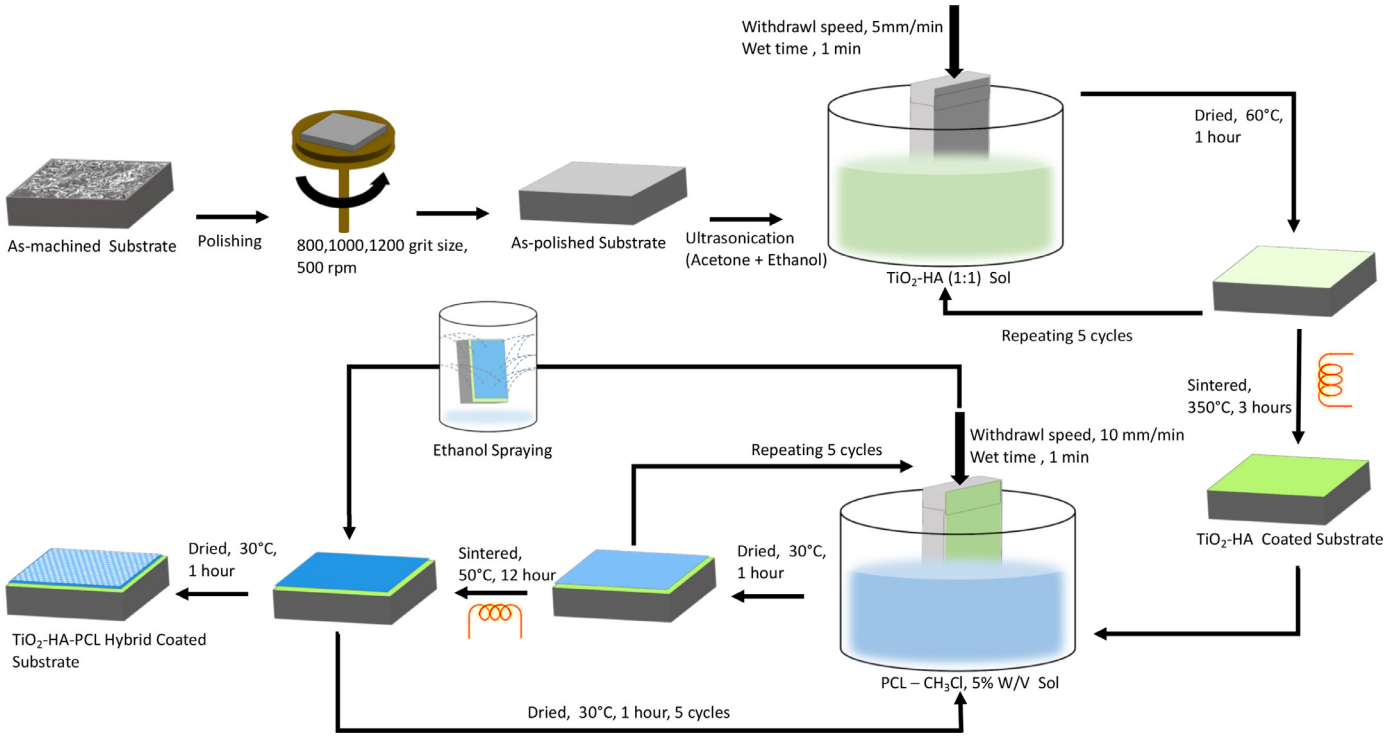

Fig. 2. Schematic representation of creating TiO_2–HA and TiO_2–HA–PCL hybrid coatings on ZM21 Mg substrate.

was measured. The corroded surfaces were examined using SEM-EDS.

2.5. Hydrogen evolution test

The amount of hydrogen evolution was measured upto 168 h. The setup consisted of sample placed below an inverted funnel placed beneath graduated burette under similar immersion conditions of weight loss study [43]. The hydrogen evolution rate V_H (ml/cm^2/day), was quantified as $V_H = \frac{V}{AxT}$, where V is the volume of hydrogen gas (ml), A is the exposed area (cm^{-2}) and T is the exposure time in days [44]. The pH of SBF was recorded after every 24 h.

3. Results and discussion

3.1. Surface analysis

The surface roughness of the as-machined and as-polished ZM21 samples was measured by surface roughness tester. The surface finish of as-machined sample is described by the maximum height of the profile (R_t= 23.180 μm), arithmetic average roughness (R_a= 3.934 μm) and the root mean square roughness (R_q= 5.012 μm). In comparison, as-polished sample has R_t=2.661μm, R_a= 0.228 μm and R_q= 0.340 μm. This indicated the level of improvement in the surface finish achieved by polishing after machining. The SEM micrograph of as-machined sample is shown in Fig. 3(a).The machined surface consists of overlapped craters (of diameter 70–100 μm) formed due to bombardment of ions generated by repetitive sparking and collapsing of vapors bubble causing melting and evaporation of material. Quick heating and cooling effect in WEDM causing re-solidification of melted material resulting into micro cracks and pores on machined surface. SEM micrograph of as-polished sample is shown in Fig. 4(a). The craters and perturbances have been rubbed off completely. The EDS spectrum were obtained for as-machined and as-polished samples. In as-machined sample, the corresponding amount of Mg, Zn, Mn and O was found to be 75.80, 0.00, 1.96 and 22.24 (inat%, as given in Fig 3(b) and in as-polished sample, it was found to be 98.69, 1.17, 0.14 and 0.00 (in at% as shown in Fig. 4(b). The presence of appreciable amount of O in as-machined sample inferred the formation of oxides of Mg and Mn on the surface. The EDS results (Fig. 4(b)) also revealed that the oxides formed during WEDM were removed on polishing.

The SEM micrograph of TiO_2–HA composite coating is shown in Fig. 5(a.i). It was found that coating was uniform but it consisted of a small number of micro-cracks and pits. The internal stresses and small amount of shrinkage during heat treatment of coating could possibly result into micro-cracks and pits, respectively [45,46]. The micro-cracks and the pits can develop potential sites for the penetration of electrolyte and subsequently for activating corrosion process. Fig. 5(b.i) shows the surface morphology of TiO_2–HA–PCL hybrid coating. Unlike TiO_2–HA coating, the TiO_2–HA–PCL coating was more homogeneous having micro-pores of 2 to

Please cite this article as: N. Singh, U. Batra, K. Kumar et al., Investigating TiO2–HA–PCL hybrid coating as an efficient corrosion resistant barrier of ZM21 Mg alloy, Journal of Magnesium and Alloys, https://doi.org/10.1016/j.jma.2020.08.003

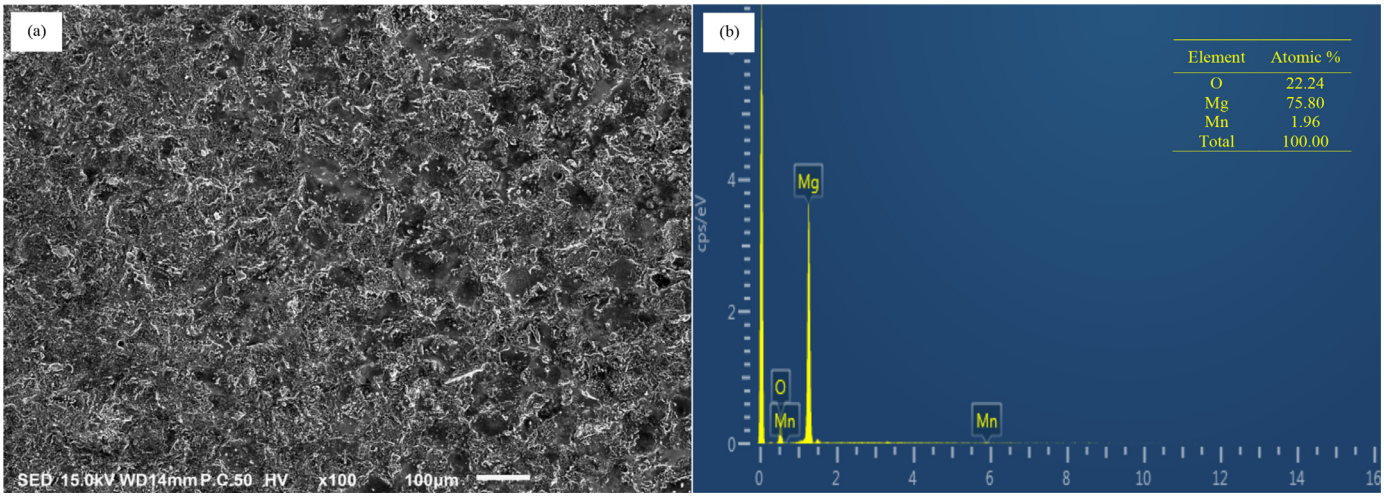

Fig. 3. SEM and EDX analysis of as-machined ZM21 substrate.

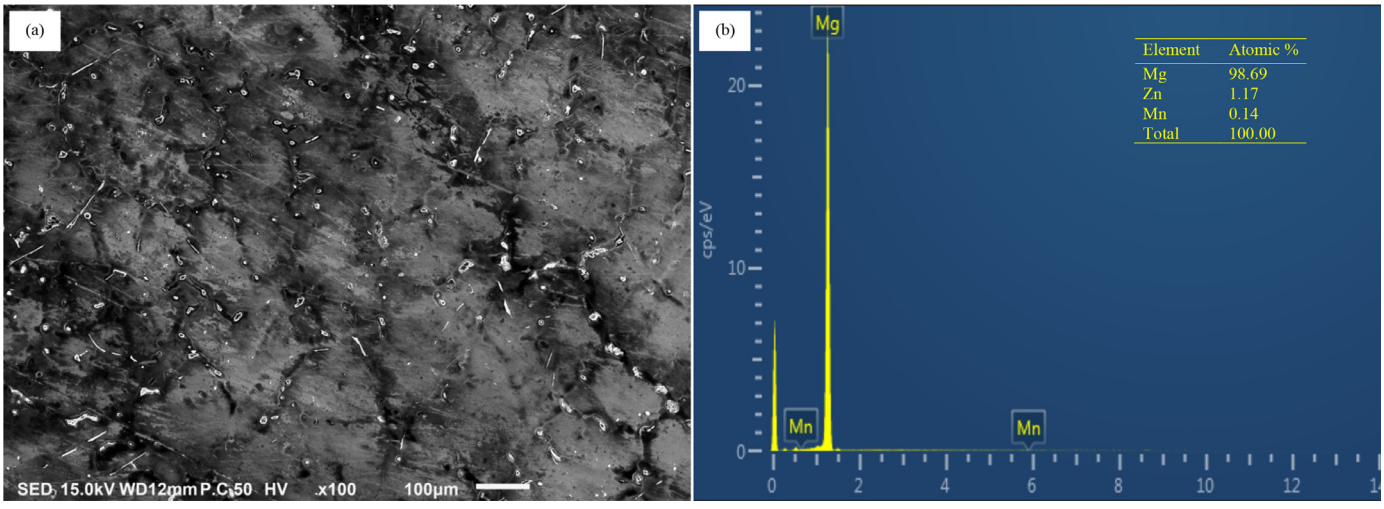

Fig. 4. SEM and EDX analysis of as-polished ZM21 substrate.

5 µm size and free of micro-cracks and pits. EDS spectra were obtained from TiO_2–HA as well as TiO_2–HA–PCL coatings. In TiO_2–HA coating, the corresponding amounts of Mg, Ti, Ca, P and O were found to be 5.17, 5.53, 15.78, 12.09 and 61.42 (in at%, as given in Fig. 5 (a.ii). The ratios Ca/P, (Ca+Mg) /P and Mg/Ca were calculated from the EDS results, these were found to be 1.30, 1.73 and 0.32 respectively. The stoichiometric ratio Ca/P in hydroxyapatite is 1.67 [47]. In the present work, the Ca/P ratio was lesser than 1.67 implying that the HA is calcium deficient. Moreover, the ratio (Ca+Mg)/P was more than 1.67 suggesting that Mg could have leached out from the Mg alloy substrate through the micro-cracks and pits in the TiO_2–HA coating.

In TiO_2–HA–PCL coating, the corresponding amounts of Mg, Ti, Ca, P and O were found to be 8.83, 0.00, 10.97, 9.14 and 69.28 (in at%) as shown in Fig. 5(b.ii). In EDS spectra of TiO_2–HA–PCL coating titanium was absent. It suggested that Ti from the TiO_2–HA layer did not interact with the PCL layer. However, presence of Mg, Ca, and P in EDS spectra of TiO_2–HA–PCL coating indicated that there was an interaction of PCL with HA from the TiO_2–HA layer as well as Mg from the substrate. The ratios Ca/P, (Ca + Mg) /P and Mg/Ca from the EDS spectra of TiO_2–HA–PCL coating were 1.20, 2.16 and 0.80, respectively. In comparison with TiO_2–HA coating, the lower Ca/P ratio and higher (Ca + Mg) /P and Mg/Ca ratios in TiO_2–HA–PCL coatings seemed to suggest that more amount of Mg leached out from the substrate during the formation of PCL layers which interacted with HA of TiO_2–HA layers and PCL of outer layer. Since the amounts of Mg as well as O in TiO_2–HA–PCL coatings are higher than in TiO_2–HA coatings, that suggests formation of MgO due the interaction of Mg with O of PCL. The SEM micrographs of the cross sections of TiO_2–HA coating and TiO_2–HA–PCL coating are shown in Fig. 6. It was revealed that the thickness of TiO_2–HA coating was 14–20 µm (Fig. 6a) whereas, TiO_2–HA–PCL hybrid coating comprised 14–20 µm of TiO_2–HA inner layer and 49–52 µm of PCL outer layer (Fig. 6b).

The formation of various bonds in TiO_2–HA coating and TiO_2–HA–PCL coating was confirmed by using FTIR spec-

Please cite this article as: N. Singh, U. Batra, K. Kumar et al., Investigating TiO2–HA–PCL hybrid coating as an efficient corrosion resistant barrier of ZM21 Mg alloy, Journal of Magnesium and Alloys, https://doi.org/10.1016/j.jma.2020.08.003

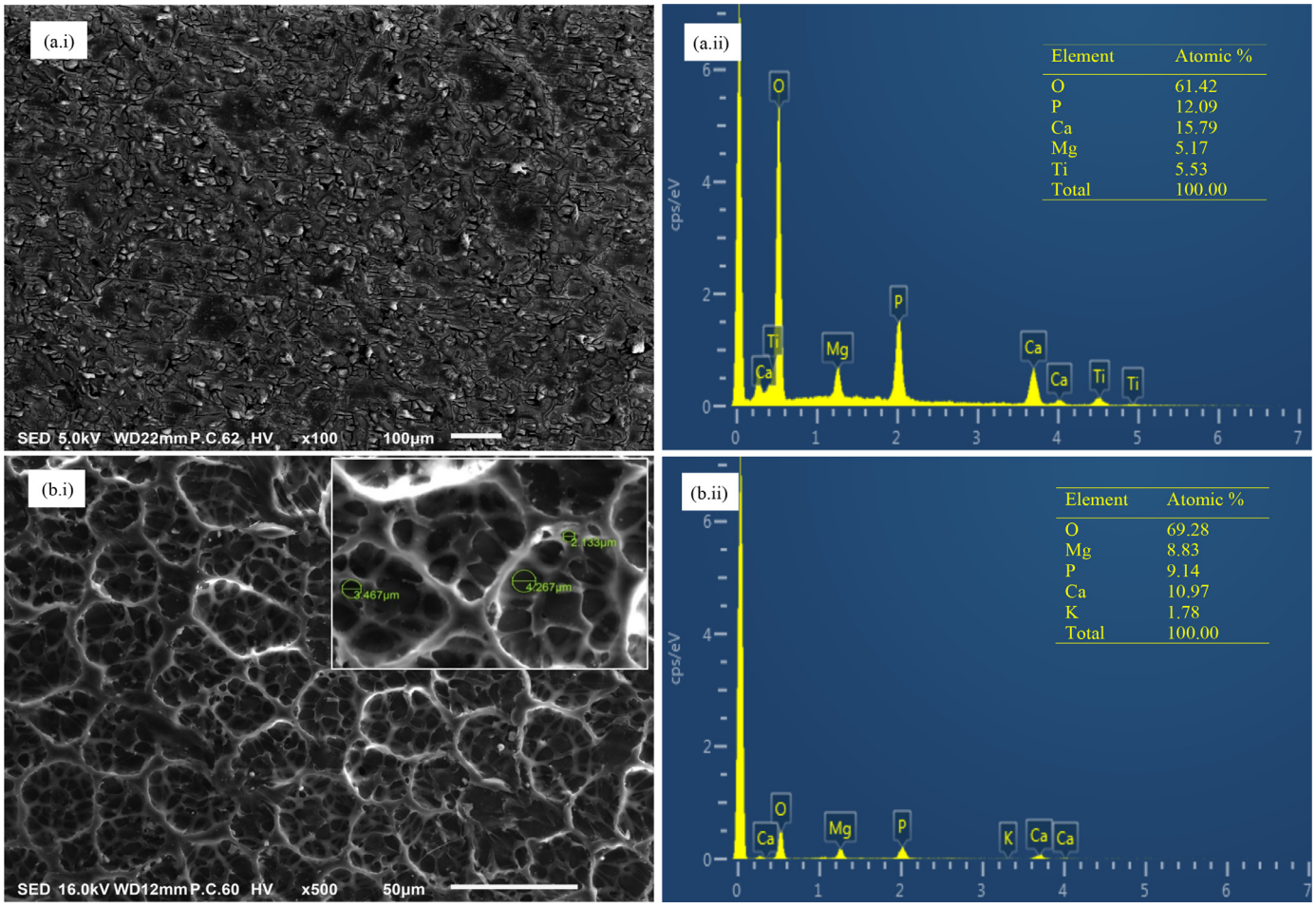

Fig. 5. SEM and EDX analysis of (a) TiO_2–HA coating and (b) TiO_2-HA–PCL hybrid coating.

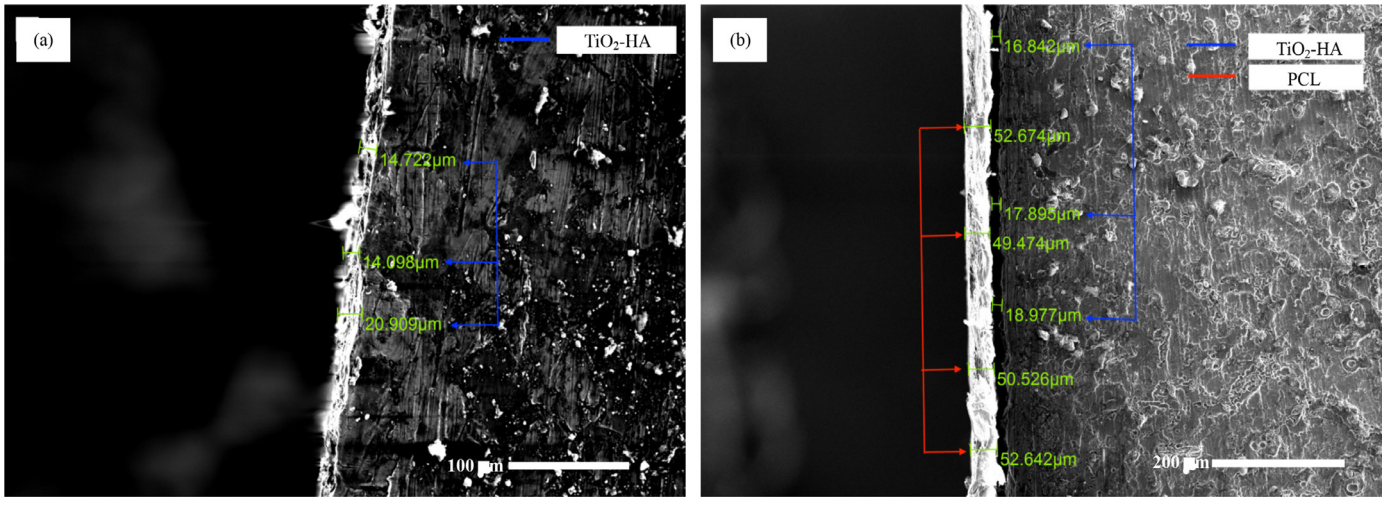

Fig. 6. SEM micrographs from the cross sections of (a) TiO_2–HA coating and (b) TiO_2–HA–PCL hybrid coating.

troscopy (Fig. 7). The peaks observed in the FTIR spectra of TiO_2–HA coating at 3443 cm^{-1} was of hydroxyl group stretching frequency. The bending vibrations at 1631 cm^{-1} was due to H_2O and Ti–OH. The PO_4^{3-} groups of HA crystal exhibits peaks at 1038–1093 cm^{-1} due to asymmetric stretching (ν_3 and ν_4) and the peaks at 564 cm^{-1} due to bending mode [35] . The peak obtained at 1384 cm^{-1} was due to Ti-O bonds which also overlaps with band of CO_3^{2-} having formed due to reaction of OH^- with CO_2 from air [48]. The band at 615 cm^{-1} was due to TiO_2. On comparing with FTIR of pure TiO_2 and pure HA, it was found that the FTIR

Please cite this article as: N. Singh, U. Batra, K. Kumar et al., Investigating TiO2–HA–PCL hybrid coating as an efficient corrosion resistant barrier of ZM21 Mg alloy, Journal of Magnesium and Alloys, https://doi.org/10.1016/j.jma.2020.08.003

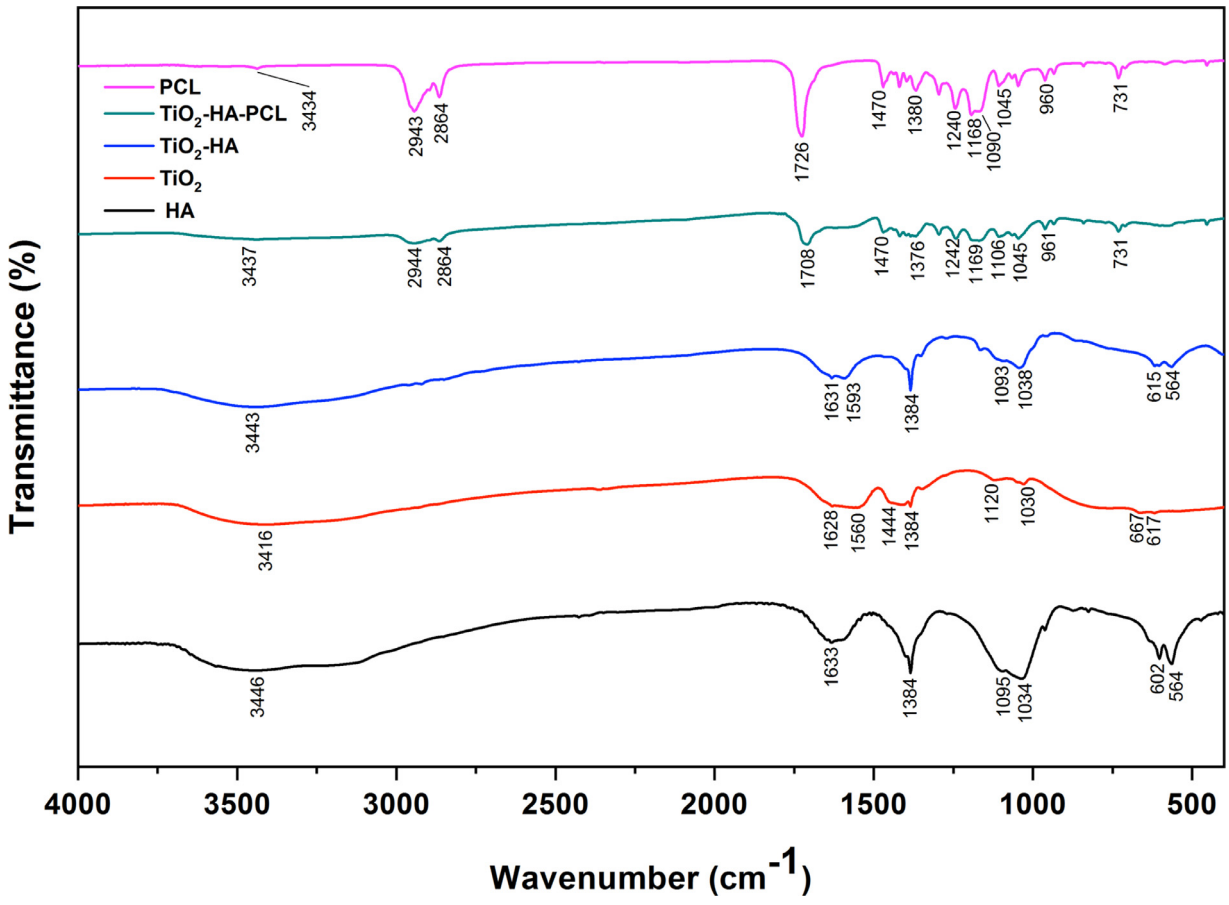

Fig. 7. FT-IR spectra of HA, TiO_2, TiO_2–HA, TiO_2–HA–PCL hybrid coating and pure PCL.

spectra of TiO_2–HA coating has peaks of TiO_2 and HA only (Fig. 7).

In the TiO_2–HA–PCL hybrid coating, the Peaks observed at 2944 cm^{-1} and 2864 cm^{-1} attributes asymmetric and symmetric stretching of CH_2. The absorption peak at 1708 cm^{-1} was due to the stretching vibration of carbonyl group of PCL. The peak observed at 1470 cm^{-1} and 1376 cm^{-1} were related to the methylene C–H bending and C–H in plane scissoring mode respectively [49] . The peaks at 1169 cm^{-1} and 1242 cm^{-1} were attributed to C–O-C symmetric and asymmetric stretching of PCL amorphous phase. The characteristic peaks corresponding to CH_2 bending vibrations were observed at 1045 cm^{-1}, 961 cm^{-1} and 731 cm^{-1} were ascribed to O–C vibrations. The peak at 671 cm^{-1} was due to TiO_2. When compared with FTIR spectra of pure PCL, it was found that the peak at 1726 cm^{-1} in PCL has been shifted to 1708 cm^{-1} in the TiO_2–HA–PCL hybrid coating {i.e. $\Delta\nu$ (C=O) =18 cm^{-1}}. The measure of this shift signifies the occurrence of hydrogen bonding between HA and PCL as shown in Fig. 7 [50–52].

As shown in Fig. 8, In TiO_2–HA spectra characteristic peaks of TiO_2 appearing at 2θ of 25.38°, 37.97°, 48.06°, 53.25°, 55.10°, 62.77°, 68.88°, 70.17° and 75.29° corresponds to (011), (004), (020), (015), (121), (024), (116), (220) and (125) crystal planes (JCPDS card no. 96-900-9087). HA peaks appearing at 2θ of 25.38°, 31.99°, 33.05°, 48.06°, 49.54°, 53.25° corresponds to (002), (211),(112),(132), (213) and (004) crystal planes (JCPDS card no. 96-900-2217). MgO peaks (JCPDS card no. 96-901-3222) detected at 2θ of 37.97°, 62.77°, 75.29° corresponds to (111), (022), (113) crystal planes. The presence of TiO_2, HA and MgO phases suggested that the coating has interaction with Mg ions from substrate. In the XRD pattern of TiO_2–HA–PCL hybrid film, the presence of orthorhombic PCL was observed at values of $2\theta = 21.2°$, 22° and 23.5° corresponding to planes (110), (111), (200) respectively. These peaks attributed the intermolecular interaction between polymer side chains due to the hydrogen bonding [53]. TiO_2 peaks are observed at 2θ of 25.26°, 38.00°, 47.98°, 53.93°, 54.97°, 62.59°, and 75.03° corresponds to (011), (004), (020), (015), (121), (024) and (125) crystal planes. HA peaks seen in the hybrid film at 2θ of 25.26°, 31.87°, 47.98°, 53.93° correspond to (002), (211), (132) and (004) crystal planes. MgO peaks in hybrid coating is detected at 2θ of 35.98°, 43.43°, 62.59°, 75.03° corresponds to (111), (002), (022), (113) crystal planes. This implied that the coating has interacted with the Mg from the substrate.

The wettability of SBF with TiO_2–HA coating and TiO_2–HA–PCL coatings on the ZM21 alloy surface was evaluated by means of contact angle (CA) measurement as shown in Fig. 9. The CA value of as-machined (56°) and as-polished (53.9°) surfaces are comparable. The TiO_2–HA coating demonstrate a higher CA value (60.7°) as compared as-

Please cite this article as: N. Singh, U. Batra, K. Kumar et al., Investigating TiO2–HA–PCL hybrid coating as an efficient corrosion resistant barrier of ZM21 Mg alloy, Journal of Magnesium and Alloys, https://doi.org/10.1016/j.jma.2020.08.003

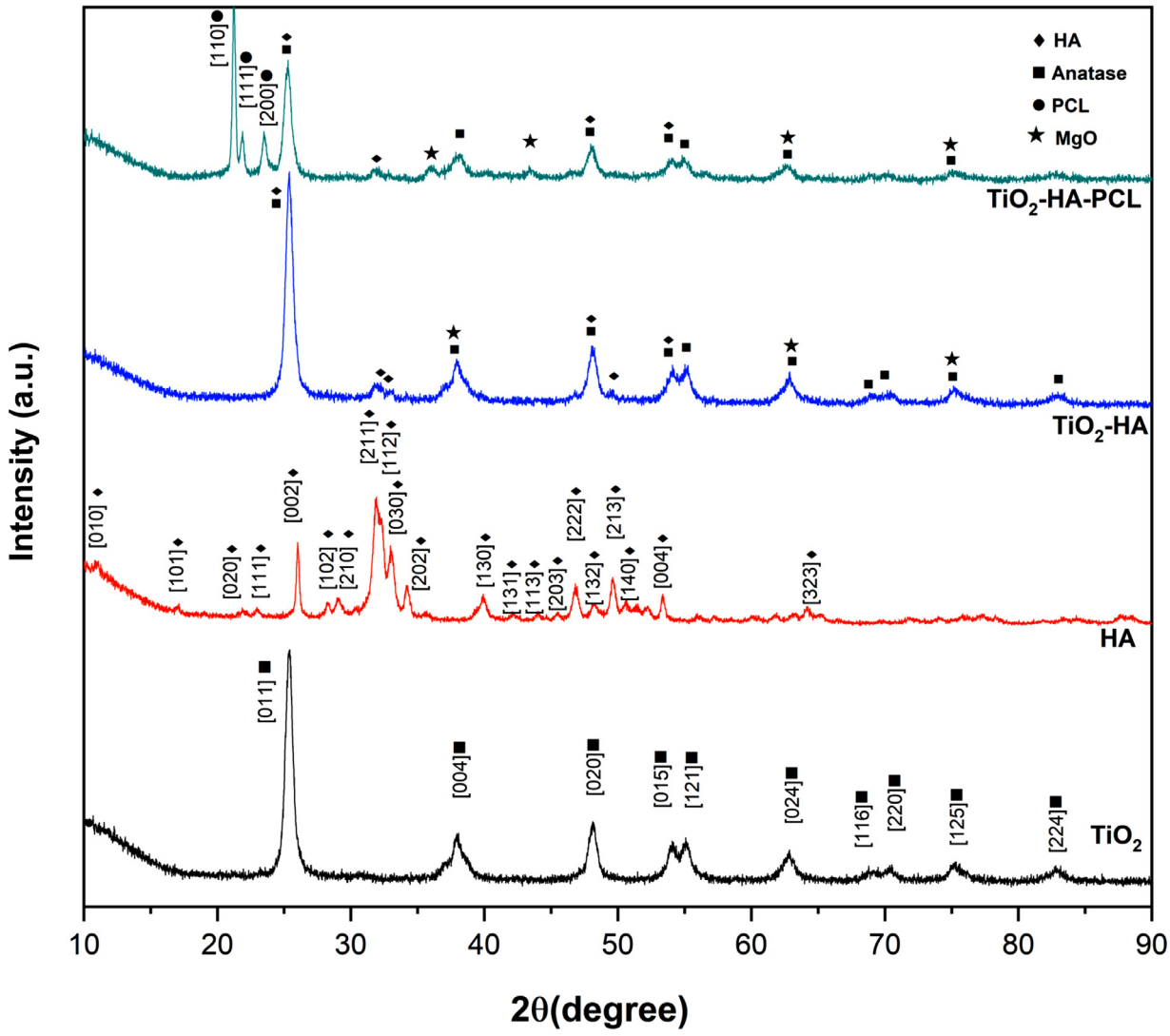

Fig. 8. XRD analysis of TiO_2, HA, TiO_2–HA coating & TiO_2–HA–PCL hybrid coating.

polished substrate. However, the TiO_2–HA–PCL hybrid coating has still higher CA value of 82.5°.

3.2. Scratch testing

Fig. 10 shows the scratch morphology and adhesion between the as-polished ZM21 Mg alloy substrate with PCL (Fig. 10a), TiO_2–HA coating (Fig. 10b) and TiO_2–HA–PCL hybrid coating (Fig. 10c). Fig 10d presents the load vs sliding distance graphs for TiO_2–HA and TiO_2–HA–PCL hybrid coatings. It was found that the TiO_2–HA–PCL hybrid coating was able to bear a critical load of 5.936 N which is nearly 1.4 times higher for TiO_2–HA which could bear only 4.159 N. The critical load borne by the outer most layer in hybrid coating comprising PCL was 3.729 N. According to the literature, adhesion strength values between Mg alloy and various coatings have been reported as 1.8 N for PCL [52], 1.35 N for TiO_2–PCL [54], 2.2 N HA–PCL [55]. For the sake of comparison, PCL layer was directly deposited on ZM21 Mg substrate and it displayed an adhesion strength of 2.195 N (Fig. 10a). After 28 days of immersion in SBF, the adhesion strength decreased by 28.38%, 27.69% and 15.11%, respectively, for PCL coating (Fig. 10e), TiO_2–HA coating (Fig. 10f), TiO_2–HA–PCL hybrid coating (Fig. 10g). The results from the ASTM tape adhesion test on the as deposited coatings displayed adhesion grades of 2B, 3B and 4B respectively for PCL coating (Fig. 11a), TiO_2–HA coating (Fig. 11b), TiO_2–HA–PCL hybrid coating (Fig. 11c) which decreased to 1B, 2B and 3B, respectively, after 28 days of immersion in SBF. Obviously, the TiO_2–HA–PCL hybrid coating displayed significantly high adhesion strength with Mg alloy as compared with other similar coatings reported in literature so far. The close examination of the results of FTIR and scratch resistance revealed that interfacial interaction happening between the organic and inorganic matrices of TiO_2–HA–PCL hybrid coating.

Each HA unit cell in the TiO_2–HA layer consists of two OH groups as strong hydrogen bonding sites, which could result into good interfacial bonding between OH groups of HA and =O sites of PCL as shown schematic diagram in

Please cite this article as: N. Singh, U. Batra, K. Kumar et al., Investigating TiO2–HA–PCL hybrid coating as an efficient corrosion resistant barrier of ZM21 Mg alloy, Journal of Magnesium and Alloys, https://doi.org/10.1016/j.jma.2020.08.003

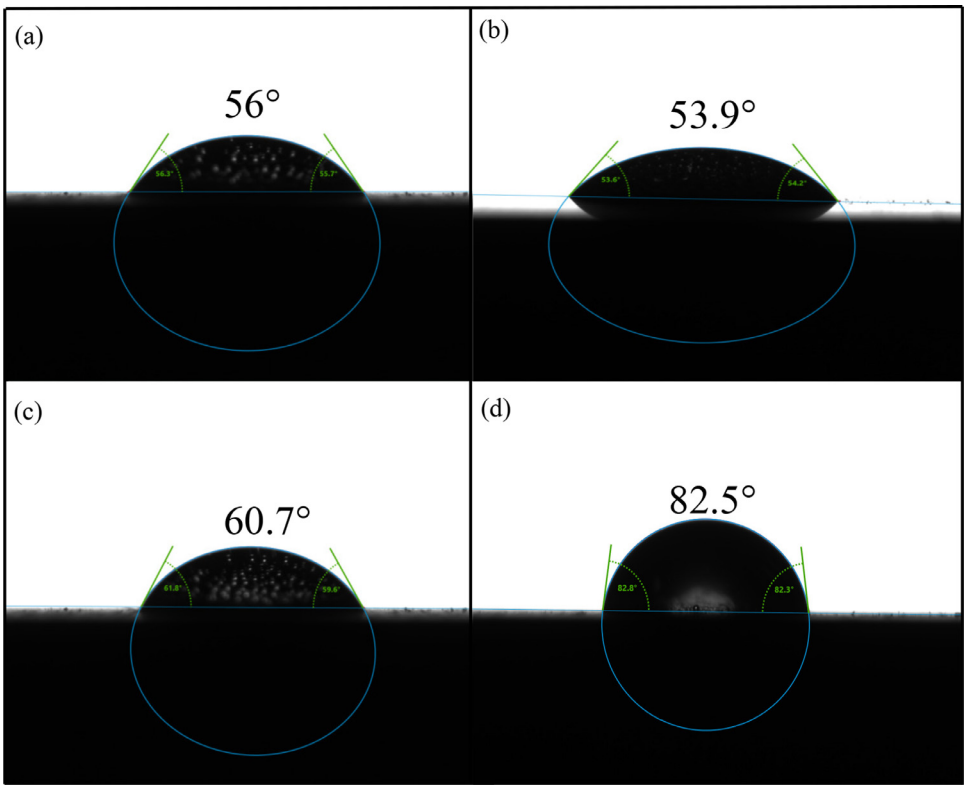

Fig. 9. Contact angles of SBF on the surface of (a) as-machined, (b) as-polished, (c) TiO_2–HA coated (d) TiO_2–HA–PCL hybrid coated ZM21 Mg alloy.

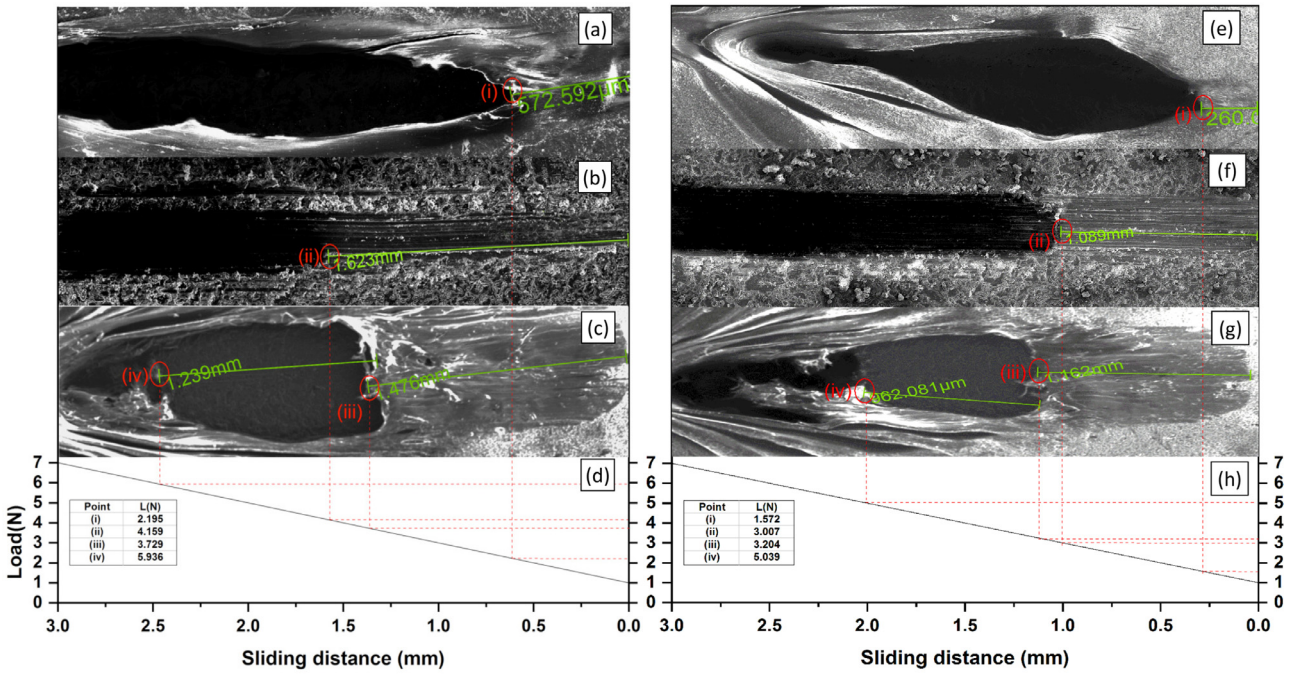

Fig. 10. Scratch morphology of (a) PCL, (b) TiO_2–HA coating, (c) TiO_2–HA–PCL hybrid coating, (d) load vs sliding distance graph before immersion and (e) PCL, (f) TiO_2–HA coating, (g) TiO_2–HA–PCL hybrid coating and (h) Load vs sliding distance graph after immersion in SBF for 28 days.

Please cite this article as: N. Singh, U. Batra, K. Kumar et al., Investigating TiO2–HA–PCL hybrid coating as an efficient corrosion resistant barrier of ZM21 Mg alloy, Journal of Magnesium and Alloys, https://doi.org/10.1016/j.jma.2020.08.003

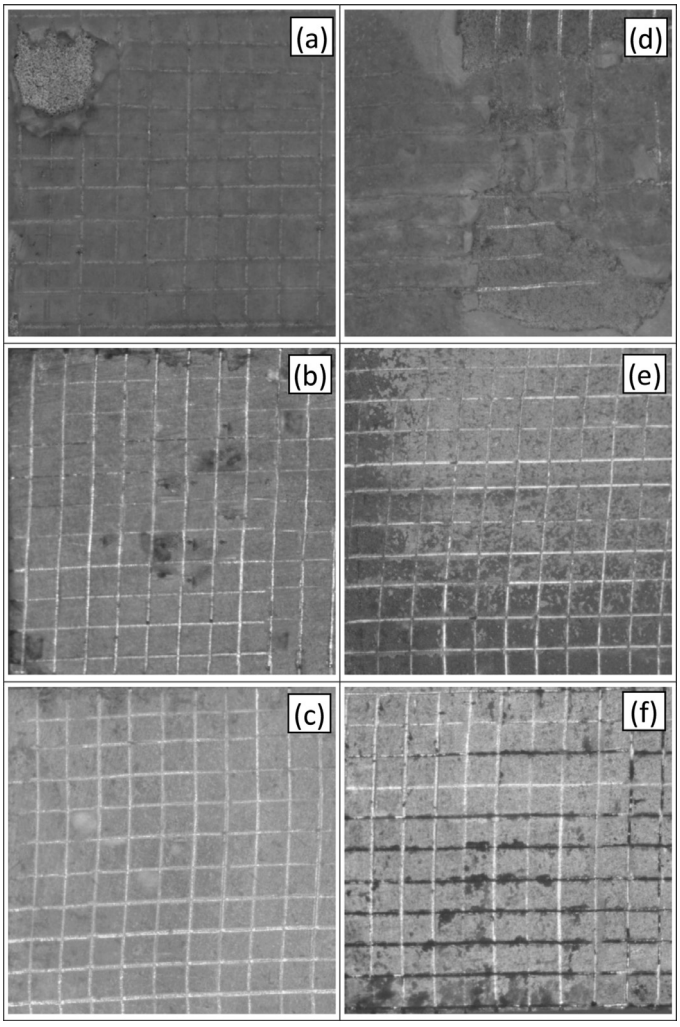

Fig. 11. Tape test results of (a) PCL, (b) TiO_2–HA coating, (c) TiO_2-HA–PCL hybrid coating before immersion and (d) PCL (e) TiO_2–HA coating (f) TiO_2-HA–PCL hybrid coating after immersion in SBF for 28 days.

Fig. 12(i) [56]. Besides, the electrostatic interaction between Mg^{+2} and =O sites of PCL in the manner shown in Fig. 12(ii) [54]. This is supported by the EDS results that show the presence of Mg in the TiO_2–HA layer. Both the hydrogen bonding provided by OH groups of TiO_2–HA layer and Vander Walls attraction due to Mg gives combined effect to provide strong interfacial bonding between TiO_2–HA and PCL layers in hybrid coating.

Besides, our observation of the EDS results on the higher amount of Mg present in TiO_2–HA–PCL coating than in TiO_2–HA coating seems to suggest that the PCL in the former makes direct contact with the Mg substrate through the pores or cracks in the intermediate TiO_2–HA layer as shown in Fig. 12 (iii). In order to understand the phenomena, PCL was coated directly on as-polished substrate. PCL has poor oxygen weight ratio in its molecular structure, thus interfacial bonding is mainly dominated by electrostatic interaction by means of Vander walls forces instead of hydrogen bonding. Vander walls interaction are generally weaker than hydrogen bonding. However, few hydrogen bonding sites are available but they are very less in number. Such kind of weak electrostatic interaction and poor hydrogen bonding of PCL with Mg resulted into adhesion strength of 2.195 N as compared to adhesion strength of 3.729 N of PCL layer over TiO_2–HA coating in hybrid coating.

3.3. Electrochemical measurements

Fig. 13a shows the potentiodynamic polarization (PDP) curves of ZM21 samples obtained after different types of processes as-machined, as-polished, as-TiO_2–HA coated and as-TiO_2–HA–PCL hybrid coated samples. According to the Table 2, the corrosion potential (E_{corr}) of as-machined, as-polished, TiO_2–HA coated samples were more negative than for as-TiO_2–HA–PCL hybrid coated sample. The polishing of as-machined samples shifted the E_{corr} to the positive direction (−1.444 V to −1.395 V), TiO_2–HA coating shifted it even further (−1.017 V). TiO_2–HA–PCL hybrid coating displayed additional jump in E_{corr} to −0.407 V. This positive shift implies that TiO_2–HA composite coating and TiO2-HA–PCL hybrid coating retarded the corrosion of as-polished sample in SBF. A breakdown down potential is observed at 0.56±0.01 V in anodic branch of the PDP curve of TiO_2–HA–PCL coated sample, which seemed to suggest that it had tendency of self-healing. Cui et al. reported that occurrence of a breakdown potential in anodic branch of polarization curve suggested the self-healing capability of the coating [57]. The current density (I_{corr}) exhibited by the TiO_2–HA-PCL hybrid coating (7.31×10^{-8} A/cm^2) was significantly lower when compared with TiO_2–HA coating (4.03×10^{-4} A/cm^2) and which were further lower than observed in as-machined (2.2×10^{-3} A/cm^2) and as-polished (1.2×10^{-3} A/cm^2) samples. This suggested that hydrophobic TiO_2–HA–PCL coating effectively protected Mg alloy substrate in the SBF. The presence of a thin and compact TiO_2–HA layer was able to restrict the penetration of SBF solution and therefore resulted into lower I_{corr} than as-machined and as-polished ZM21 samples. The Nyquist plots of as-machined, as-polished and TiO_2–HA coated samples (Fig. 13b) comprised of two capacitive loops at high and medium frequency due to charge transfer resistance between substrate and corrosive media, diffusion of ions through corrosion product and coating respectively and one inductive loop at low frequency region due to adsorption processes [58]. The Nyquist plot for TiO_2–HA–PCL hybrid coated sample comprised of a capacitive loop followed by a diffusional tail which signify porous nature of coating. The impedance modulus increases at nearly 45° in low and medium frequency regions suggesting that the corrosion product formed in-between pores is highly resistant and stable [59].

The charge transfer resistance (R_{ct}) is a measure of diameter of high frequency capacitive loop [58] . The R_{ct} of TiO_2–HA–PCL was nearly 10^4 times of the value obtained for TiO_2–HA coating. In comparison the R_{ct} value for as-machined and as-polished ZM21 alloy were much smaller. The as-polished substrate presented low R_{ct} due to the formation of loose and porous protecting film such as $Mg(OH)_2$ that

Please cite this article as: N. Singh, U. Batra, K. Kumar et al., Investigating TiO2–HA–PCL hybrid coating as an efficient corrosion resistant barrier of ZM21 Mg alloy, Journal of Magnesium and Alloys, https://doi.org/10.1016/j.jma.2020.08.003

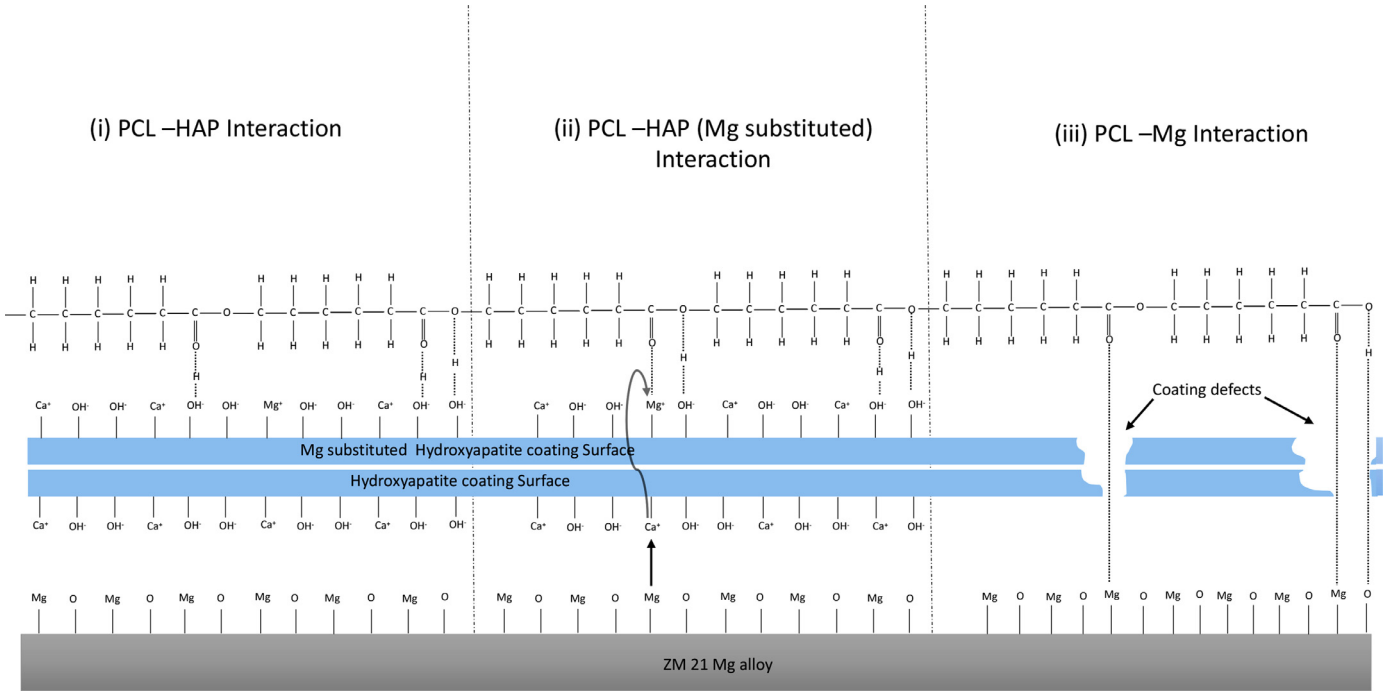

Fig. 12. Schematic illustration of electrostatic interaction between (i) PCL coating with HA, (ii) PCL coating with Mg substituted HA, (iii) PCL coating with ZM21 Mg alloy.

Table 2
Electrochemical parameters of the polarization curves in SBF.

Samples	b_a(V/dec)	b_c(V/dec)	E_{corr}(V)	I_{corr}(A/cm²)	Corrosion rate(mm/year)	Polarization resistance(Ωcm^2)
As-machined	0.942	1.634	−1.444	2.2×10^{-3}	103.700	114.415
As-polished	0.659	0.438	−1.395	1.2×10^{-3}	56.043	93.228
TiO_2–HA coated	0.337	0.378	−1.017	4.03×10^{-4}	18.409	192.382
TiO_2–HA–PCL hybrid coated	0.252	0.216	−0.407	7.31×10^{-8}	0.003	692,900

could not effectively protect the substrate against the infiltration of corrosive medium. The visibly larger R_{ct} of TiO_2–HA–PCL hybrid coated sample was due to its hydrophobic characteristics that reduced contact area with the corrosive medium.

3.4. Immersion testing

Fig. 14 shows the surfaces of samples immersed in SBF for 28 days and subsequently cleaned with chromic acid. The corroded surface of as-machined exhibited largest sizes of pits and cracks among all four types of samples. The size of pits and cracks was smaller in as-polished samples than in as-machined samples. The sizes were further lower in TiO_2–HA coated sample. In contrast the TiO_2–HA–PCL hybrid coated sample surface did not show pitting or crack formation.

Hydrogen evolution test was used to study the corrosion behavior of the samples as a function of time. Higher amount of H_2 gas evolution during implantation results in increase in pH which leads to hemolysis of cells [60]. Fig. 15(a) shows the H_2 evolution rate (HER) for the as-machined, as-polished, TiO_2–HA coated and TiO_2–HA–PCL hybrid coated samples during immersion in SBF for 7 days. Due to presence of cracks on the surface of as-machined surface and low electrochemical potential (−1.444 V), bubbles appeared as soon as the sample was immersed in SBF and the H_2 evolution rate after 24 h was 3.3 ml/cm^2/day and the corresponding pH of SBF was 7.85. During this period the degradation rate became faster and more pits appeared on the surface. After 24 h, H_2 evolution rate was found to be comparable in as-polished and TiO_2–HA coated sample. As the corrosion proceeded, the apatite formed on the surfaces and H_2 evolution was suppressed. The apatite growth was easily noticeable in TiO_2–HA coated sample than as-polished and as-machined samples. At the end of 144 h, apatite growth became so effective that the H_2 evolution rate in TiO_2–HA coating and hybrid coating sample became comparable. After 172 h, H_2 evolution increased for TiO_2–HA coated sample. It might be due to the delamination of coating layer/ corrosion product caused by evolved hydrogen. In contrast to as-machined, as-polished and TiO_2–HA coated sample, TiO_2–HA–PCL hybrid coated sample was more protected and restricted the attack of aggressive ions as no bubble appeared for first 12 h and later some bubbles were observed at isolated places. The hydrogen evolution rate was very low and sample appeared unaffected as compared to as-machined, as-polished and TiO_2–HA coated samples throughout the immersion period. Even after 168 h,

Please cite this article as: N. Singh, U. Batra, K. Kumar et al., Investigating TiO2–HA–PCL hybrid coating as an efficient corrosion resistant barrier of ZM21 Mg alloy, Journal of Magnesium and Alloys, https://doi.org/10.1016/j.jma.2020.08.003

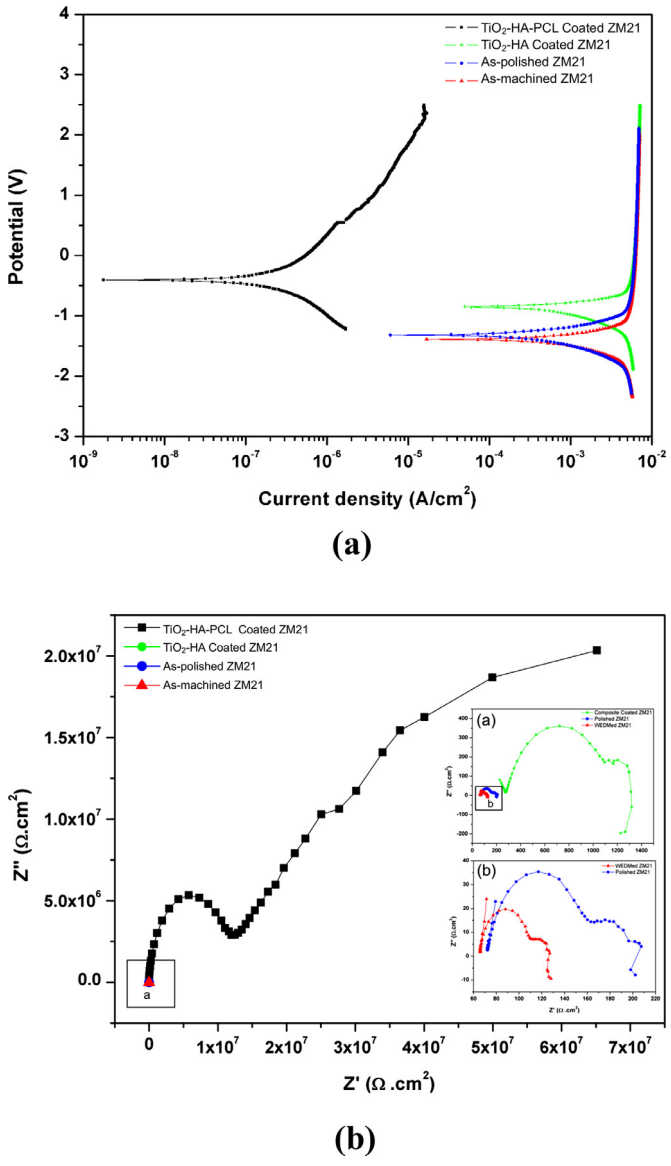

Fig. 13. Electrochemical measurments of as-machined, as-polished, TiO_2–HA and TiO_2–HA–PCL hybrid coated ZM21Mg substrate: (a) PDP curves and (b) Nyquist Plots.

the HER was 0.16 ml/cm^2/day, the pH of SBF was 7.46 and TiO_2–HA–PCL hybrid coating was intact without any sign of cracks or delamination. Fig. 15(b) shows the variation of pH of the SBF during 7 days of immersion at regular interval of 24 h for as-machined, as-polished, TiO_2–HA, and TiO_2–HA–PCL hybrid coated samples. Interestingly, the change in pH was lower for coated samples than for un-coated samples. It was significantly lower for TiO_2–HA–PCL coated sample than all other samples.

Fig. 15(c) displayed the weight loss percentage for as-machined, as-polished, TiO_2–HA, and TiO_2–HA–PCL coated samples after 28 days of immersion in SBF. The weight loss trend indicated that polishing, TiO_2–HA coating and TiO_2–HA–PCL coating has synergetic effect on corrosion protection during immersion time. The coating effectiveness can be assessed in the terms of weight loss (%) ratio for as-machined, as-polished, TiO_2–HA, and TiO_2–HA–PCL coated samples being 1: 1/2.5: 1/7: 1/9.

Fig. 16 shows the surface morphology of samples immersed in SBF for 28 days. In the as-machined sample, the corrosion product was porous and uneven. There was severe degradation of as-machined sample. As-polished sample has relatively denser and evenly distributed corrosion product on the surface. The density and evenness of the corrosion product was improved for TiO_2–HA coated sample. The corrosion product on TiO_2–HA–PCL coated sample was the most compact and evenly spread among all the samples. SEM-EDS in Fig. 17 shows the morphology and elemental analysis of corrosion product deposits. The corrosion product deposit on as-machined, as-polished and TiO_2–HA coated samples had numerous cracks and pits but the deposit on TiO_2–HA–PCL coated sample was defect free and evenly spread. According to EDS analysis, the ratios Ca/P, (Ca+Mg)/P and Mg/Ca of deposits are compared in Table 3 for the as-machined, as-polished, TiO_2–HA coated and TiO_2–HA–PCL coated samples. The atomic percentage of Ca, P and Mg elements is shown in Fig. 18.

These Ca/P values suggested the formation of calcium deficient hydroxyapatite on the surfaces. Such kind of calcium deficiencies have been reported due to the dissolution of Mg from the substrate partly replacing Ca in the apatite struc-

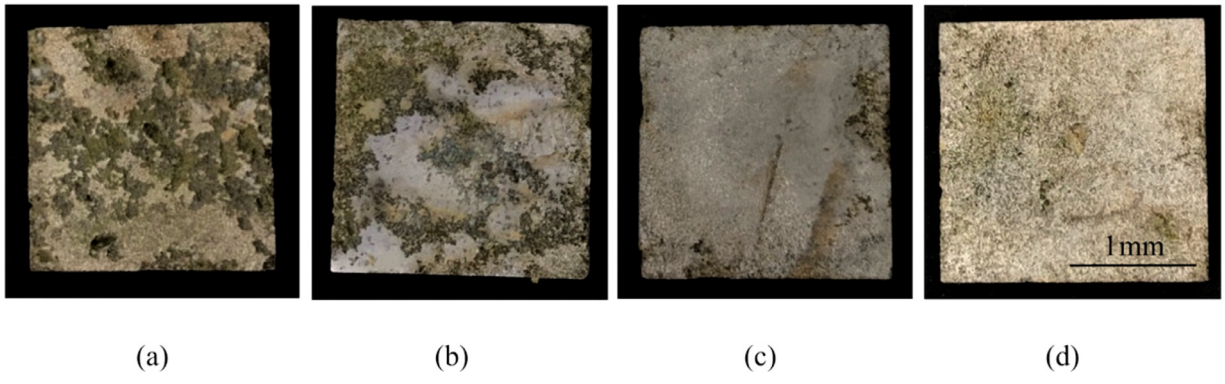

Fig. 14. Morphology comparison of the specimens; (a) as-machined, (b) as-polished, (c) TiO_2–HA coated, (d) TiO_2–HA–PCL hybrid coated ZM21 Mg samples after immersion in SBF for 28 days.

Please cite this article as: N. Singh, U. Batra, K. Kumar et al., Investigating TiO2–HA–PCL hybrid coating as an efficient corrosion resistant barrier of ZM21 Mg alloy, Journal of Magnesium and Alloys, https://doi.org/10.1016/j.jma.2020.08.003

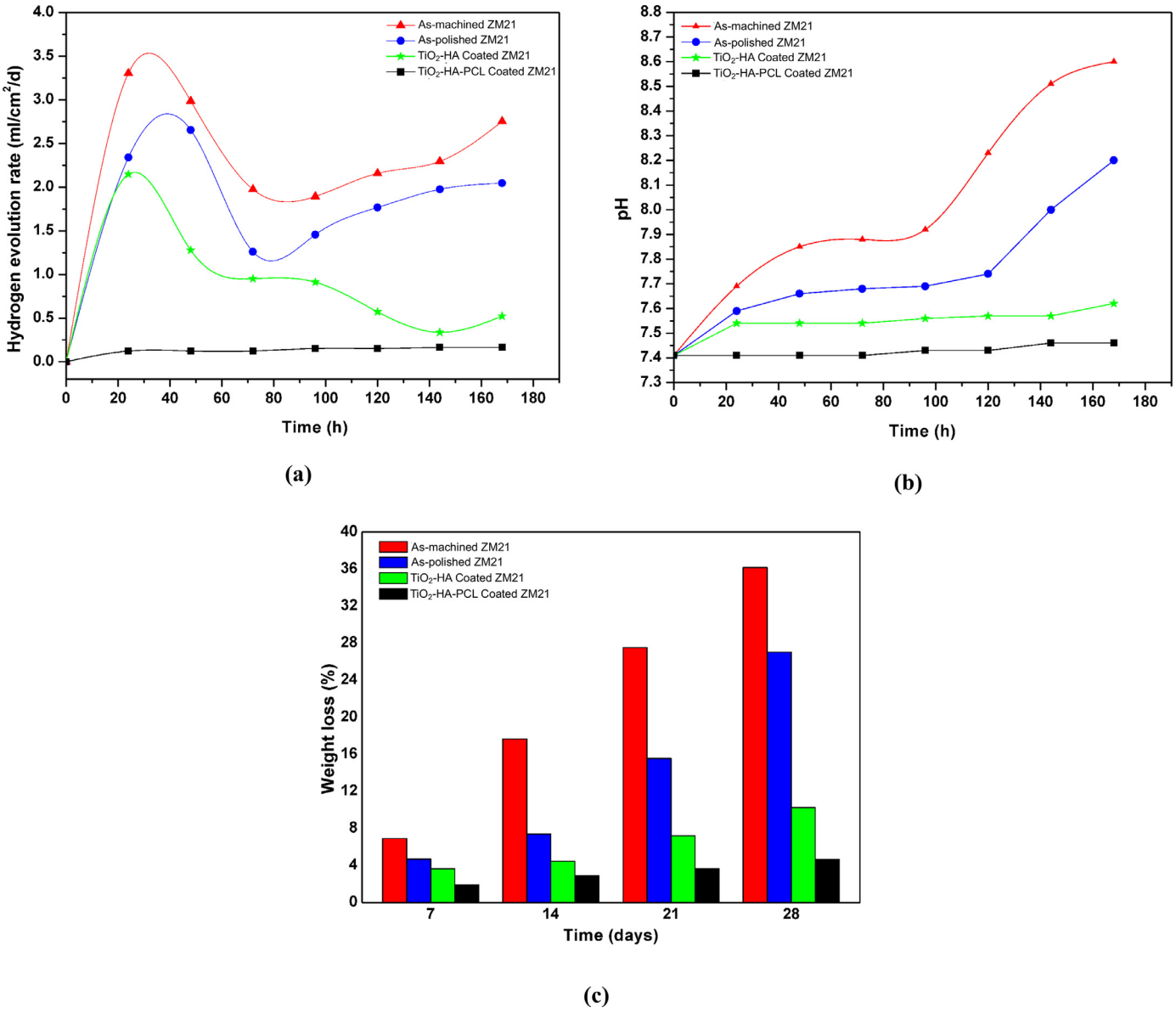

Fig. 15. Hydrogen evolution rate (a), pH change (b) and weight loss percentage (c) for as-machined, as-Polished, TiO_2–HA coated and TiO_2–HA–PCL hybrid coated ZM21 Mg samples after immersion in SBF for 28 days.

Fig. 16. Morphology comparison of the corrosion product deposited over; (a) as-machined, (b) as-polished, (c) TiO_2–HA coated and (d) TiO_2–HA–PCL hybrid coated ZM21 Mg samples after immersion in SBF for 28 days.

Please cite this article as: N. Singh, U. Batra, K. Kumar et al., Investigating TiO2–HA–PCL hybrid coating as an efficient corrosion resistant barrier of ZM21 Mg alloy, Journal of Magnesium and Alloys, https://doi.org/10.1016/j.jma.2020.08.003

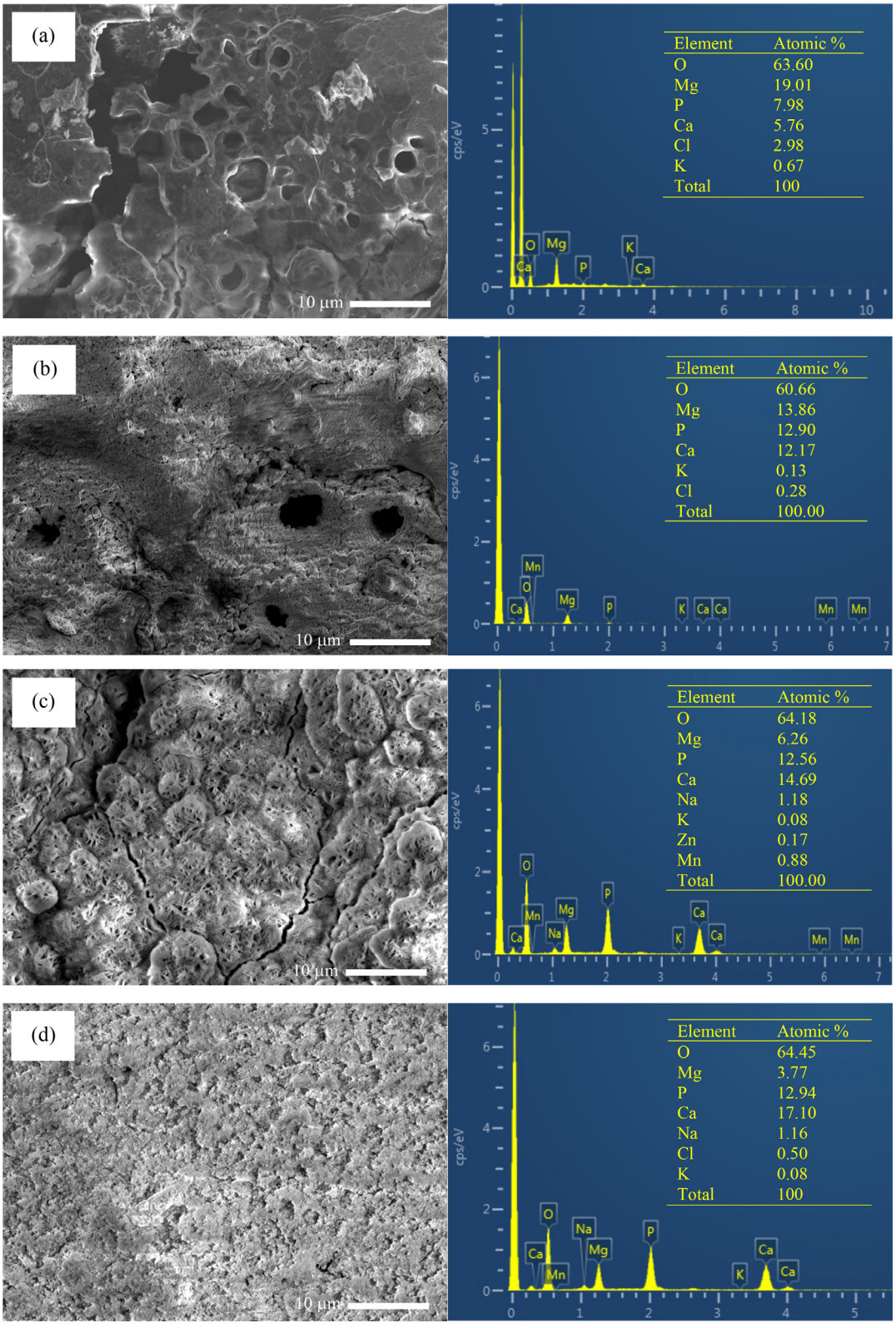

Fig. 17. SEM morphology and EDS spectra of (a) as-machined, (b) as-polished, (c) TiO_2-HA coated and (d) TiO_2–HA–PCL hybrid coated ZM21Mg samples after immersion in SBF for 28 days.

Please cite this article as: N. Singh, U. Batra, K. Kumar et al., Investigating TiO2–HA–PCL hybrid coating as an efficient corrosion resistant barrier of ZM21 Mg alloy, Journal of Magnesium and Alloys, https://doi.org/10.1016/j.jma.2020.08.003

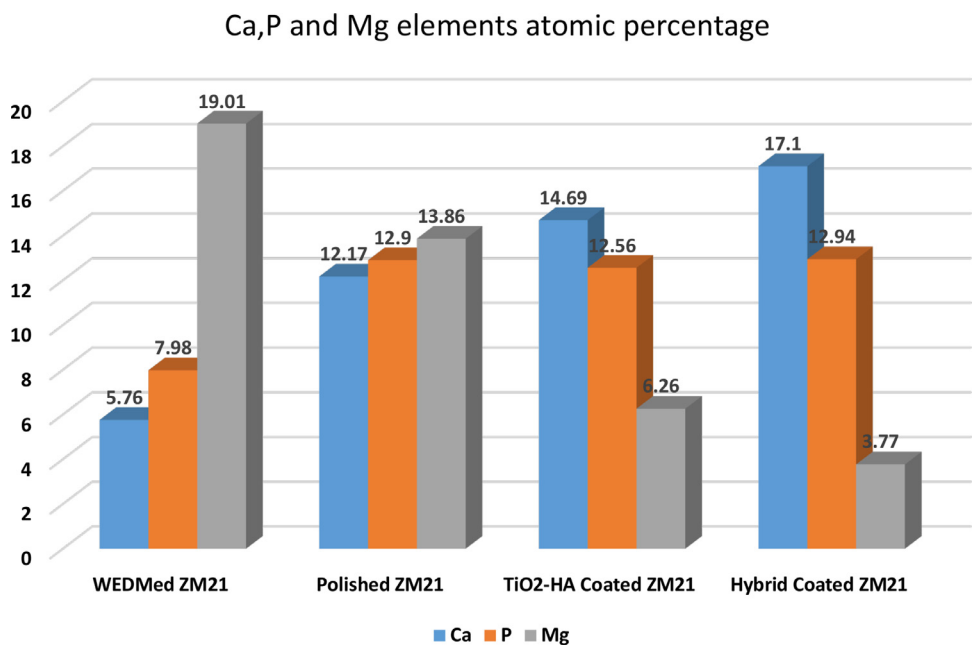

Fig. 18. Atomic percentage of Ca, P and Mg elements of as-machined, as-polished, TiO_2–HA and TiO_2-HA–PCL coated ZM21Mg substrate immersed in SBF for 28 days.

Table 3
Atomic ratios of Ca, P and Mg of corrosion product on as-machined, as-polished, TiO_2–HA coated and TiO_2–HA–PCL coated ZM21 Mg samples after immersion in SBF for 28 days.

Sample	Ca/P(at%)	(Ca+Mg)/P(at%)	Mg/Ca (at%)
As- machined	0.72	3.10	3.30
As-polished	0.94	2.01	1.13
TiO_2–HA Coated	1.16	1.66	0.42
TiO_2–HA–PCL hybrid coated	1.32	1.61	0.22

ture [61] . Thus Ca/P ratio was the related to release of Mg ions by the substrate. TiO_2–HA–PCL coating has acted as an effective barrier between SBF and substrate. The highest Ca/P ratio of 1.32 and lowest Mg/Ca ratio of 0.22 among all the samples clearly indicated that the TiO_2–HA–PCL coated sample has allowed the minimum amount of Mg ions leaching from the substrate followed by TiO_2–HA coated sample having second highest Ca/P ratio (1.16) and second lowest Mg/Ca ratio of 0.42. Since the Ca/P ratio was 0.72 and 0.94 for as-machined and as-polished samples respectively, therefore, it was inferred that the corrosion product on the bare Mg alloy surface did not offer an effective barrier. Thus more and more Mg ions continued to leach from the substrate. As a consequence, the degradation continued to result in high Mg/Ca ratios of 3.30 and 1.13 in as-machined and as-polished samples, respectively.

The FT-IR of samples immersed in SBF for 28 days were shown in Fig 19. In TiO_2–HA–PCL hybrid coated sample, the bands present at 962 cm^{-1}, 1033–1095 cm^{-1} and 565 and 603 cm^{-1} represents ν_1 PO_4^{3-}, ν_3 PO_4^{3-} , ν_4 PO_4^{3-} . Band appearance at 1596 cm^{-1} was due to the presence of lattice water, while band at 3698 cm^{-1} represents vibration modes of OH group. This represents good mapping with the HA characteristic bands. As compared to hybrid sample, continuous decrease in the intensity of PO_4^{3-} and OH^- was observed for corrosion product of TiO_2–HA, as-polished and as-machined ZM21 samples. Moreover, the broadening of ν_3 PO_4^{3-} (1033–1095 cm^{-1}) band in order of TiO_2–HA–PCL < TiO_2–HA< as-polished<as-machined ZM21 samples was observed. These effects are typically suggesting that structurally disordered Ca-Def HA is formed as corrosion product [35,62,63].

Fig. 20 showed the XRD spectra of TiO_2–HA–PCL hybrid coated, TiO_2–HA coated, as-polished and as-machined ZM21 samples immersed in SBF for 28 days. Along with characteristic peaks of HA, the presence of Mg-PO_4^{3-} compounds signified the formation of Mg substituted Ca-Def HA [64].

3.5. Corrosion mechanism

The degradation phenomena of bare Mg surface can be explained as Mg comes in contact with SBF, following reaction will occur

$$\text{Anodic: } Mg \rightarrow Mg^{2+} + 2e^- \quad (4)$$

$$\text{Cathodic: } 2H_2O + 2e^- \rightarrow 2OH^- + H_2 \quad (5)$$

$$\text{Overall: } Mg + H_2O \rightarrow Mg(OH)_2 + H_2 \quad (6)$$

The presence of Cl^- in the SBF transforms $Mg(OH)_2$ into $MgCl_2$.

$$Mg(OH)_2 + Cl^- \rightarrow MgCl_2 + OH^- \quad (7)$$

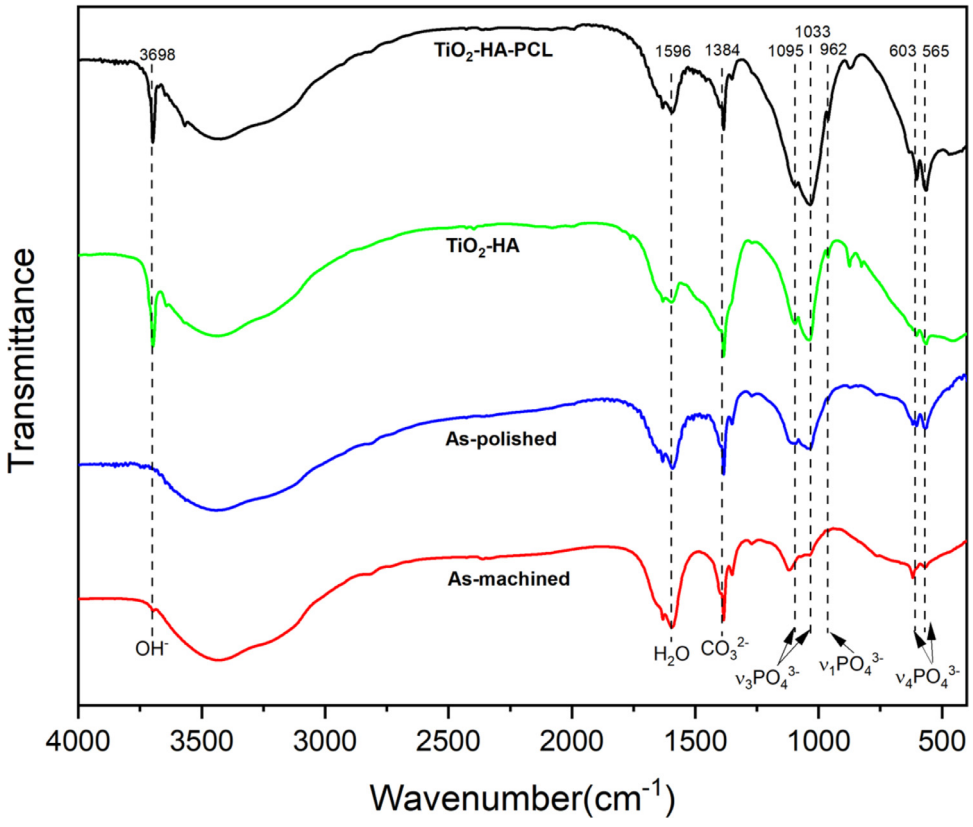

Fig. 19. FT-IR spectra of corrosion product deposited over as-machined, as-polished, TiO_2–HA coated and TiO2-HA–PCL hybrid coated ZM21 Mg samples after immersion in SBF for 28 days.

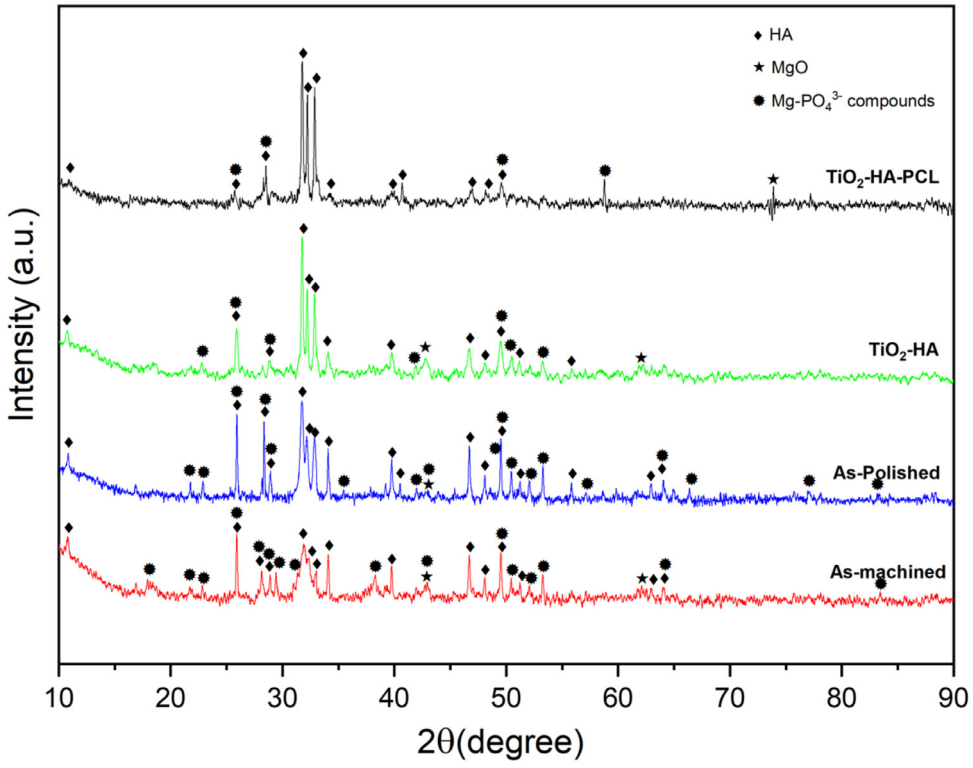

Fig. 20. XRD analysis of corrosion product deposited over as-machined, as-polished, TiO_2–HA coated and TiO_2–HA–PCL hybrid coated ZM21 Mg samples after immersion in SBF for 28 days.

Please cite this article as: N. Singh, U. Batra, K. Kumar et al., Investigating TiO2–HA–PCL hybrid coating as an efficient corrosion resistant barrier of ZM21 Mg alloy, Journal of Magnesium and Alloys, https://doi.org/10.1016/j.jma.2020.08.003

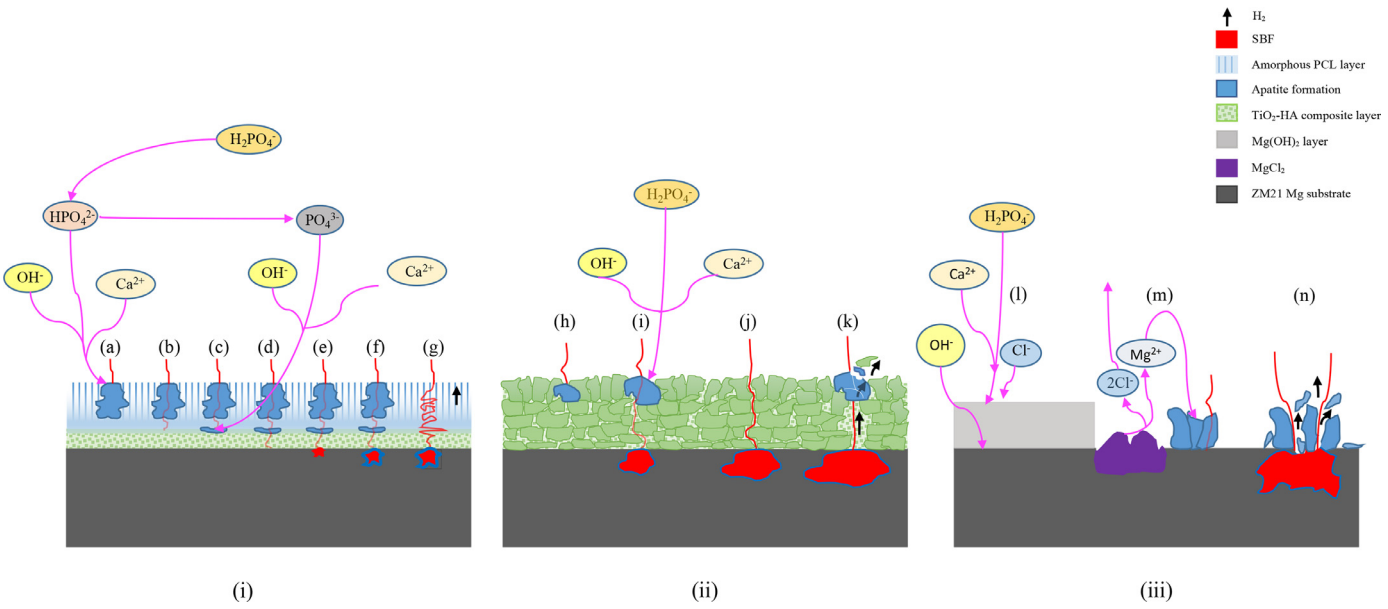

Fig. 21. Schematic illustration of the Adsorption mechanism of (i) TiO_2-HA–PCL hybrid coated, (ii) TiO_2–HA coated and (iii) as machined/polished ZM21 Mg substrate immersed in SBF.

The excess OH^- ions generated thus increase the pH of the immersed media [65]. It was observed that for as-machined substrate active corrosion was carried away from the zero hour of immersion as compared to polished sample, which show such a rise in pH nearly after 24 h of immersion. It is considered that the $H_2PO_4^-$ and HPO_4^{2-} ions from SBF transformed into PO_4^{3-} ions:

$$H_2PO_4^- + OH^- \rightarrow HPO_4^{2-} + H_2O \quad (8)$$

$$HPO_4^{2-} + OH^- \rightarrow PO_4^{3-} + H_2O \quad (9)$$

The presence of Ca^{2+} and excess of OH^- ions in SBF enables of transformation of HPO_4^{2-} and PO_4^{3-} ions into hydroxyapatite according to the following reaction

$$10Ca^{2+} + 10HPO_4^{2-} + 12OH^- \rightarrow Ca_{10}(PO_4)_6(OH)_2 + 10H_2O + 4PO_4^{3-} \quad (10)$$

$$10Ca^{2+} + 6PO_4^{3-} + 2OH^- \rightarrow Ca_{10}(PO_4)_6(OH)_2 \quad (11)$$

Ideally, HA has stoichiometric Ca/P ratio of 1.67. Fig. 17 shows that the Ca/P ratios of the corrosion product formed on the as-machined (0.72), as-polished (0.94), TiO_2–HA coated (1.16) and TiO_2–HA–PCL coated (1.32) samples immersed in SBF. Thus, Ca deficient hydroxyapatite formation has occurred as corrosion product [66–68]. The formation of Ca-deficient HA takes place by the following reaction:

$$(10\text{-}x)Ca^{2+} + 6HPO_4^{2-} + (8\text{–}2x)OH^- \rightarrow Ca_{10\text{-}x}(HPO_4)_x(PO_4)_{6\text{-}x}(OH)_{2\text{-}x} + (6\text{-}x)H_2O \quad (12)$$

Mg^{2+} ions possess most dominating bivalent cationic substitution in apatite [69]. The size of Mg^{2+} ions (0.069 nm) relatively smaller than Ca^{2+} ions (0.099 nm), which facilitates the Mg^{2+} ions to substitute Ca^{2+} ions in the apatite [70,71] . Lattice distortion caused by substitution results into poorly crystalline, highly soluble, destabilized Mg substituted Ca-deficient hydroxyapatite formation [72]. This enables the flow of electrolyte through its amorphous structure as shown in Fig. 18. Thus, Eq. (12) can be modified to show the formation as:

$$(10\text{-}x)Ca^{2+} + xMg^{2+} + 6HPO_4^{2-} + (8\text{–}2x)OH^- \rightarrow Ca_{10\text{-}x}Mg_x(HPO_4)_x(PO_4)_{6\text{-}x}(OH)_{2\text{-}x} + (6\text{-}x)H_2O \quad (13)$$

However, as a consequence of reduced interaction between the Mg substrate and SBF for the coated samples, the release of Mg^{2+} from the substrate is significantly reduced resulting in the formation of corrosion products having higher Ca/P ratio and effective corrosion barrier.

The mechanism of effective corrosion resistance displayed by the hybrid coating is suggested as follows. The electrolyte first enters into the topological pores of PCL layer where the corrosion product formation initiates Fig. 21(i.a). The corrosion product formed within the pores help the interlocking of pores from many coating layers [73] . Thus, hydroxyapatite so formed was not only stable structurally but also acts as obstacle to delay the advancing aggressive ions. Few aggressive ions which manage to escape through the apatite layer are encountered with the permeable matrix of the PCL Fig. 21(i.b). The restricted number of ions which manage to diffuse through the PCL matrix reached at the underneath bioactive TiO_2–HA composite layer. Apatite formation may start in the pores and cracks of the TiO_2–HA composite layer due to the presence of HA there, which acts yet another barrier to the movement of ions Fig. 21(i.c). As a result of barriers at various layer only a few outnumbered aggressive ions

Please cite this article as: N. Singh, U. Batra, K. Kumar et al., Investigating TiO2–HA–PCL hybrid coating as an efficient corrosion resistant barrier of ZM21 Mg alloy, Journal of Magnesium and Alloys, https://doi.org/10.1016/j.jma.2020.08.003

can succeed to reach to the Mg substrate Fig. 21 (i. d). Once the aggressive ions reach the substrate, an active corrosion starts here according to reaction (1) and (2) which results into evolution of H_2 gas Fig. 21(i.e,f). Evolved H_2 gas easily escapes out from the pores in the TiO_2–HA layer and surface pores of the PCL film thereby causing little or no damage or delamination of the coating. The intricate route accompanied by multilevel barriers for the flow of electrolyte, greatly delays the interaction between Mg substrate and aggressive ions Fig. 21(i.g). In the case of TiO_2–HA coating, the electrolyte can reach the substrate either diffusing though corrosion product Fig. 21 (ii.i) or by throughout pores/cracks in the composite layer Fig. 21 (ii.j). Thus, the corrosion process starts fairly early in TiO_2–HA coated sample than in TiO_2–HA–PCL coating. Additionally, the escaping H_2 cause cracks in the corrosion product Fig. 21 (ii.k). In case of as-machined and as-polished ZM21Mg substrates, no such effective corrosion resistance mechanism is observed. On substrate/SBF interaction, once the oxide layer formed Fig. 21 (iii.l) is deteriorated by the active corrosion. Although, apatite formation occurred on the Mg alloy surface Fig. 21 (iii.m) but it does not provide effective shielding towards aggressive ions. The corrosion product formed is highly unstable both structurally as well as chemically. The corrosion rate observed are exceedingly high that led to large volume of H_2 evolution. The abandoned H_2 evolution further cause severe damage to the corrosion product formed on surface Fig. 21 (iii.n) thereby exposing fresh Mg surface to advance corrosion.

4. Conclusions

i TiO_2–HA–PCL hybrid coatings with the top layer of interconnected microporous PCL were deposited on ZM21 alloy by sol–gel dip-coating method combined with non-solvent induced phase separation technique.
ii The adhesion strength of TiO_2–HA–PCL hybrid coating was 1.5 times more than TiO_2–HA composite coating because of bonding of PCL by hydrogen bonding with HA in addition to electrostatic bonding with the Mg substrate. The loss of adhesion strength of hybrid coating after 28 days of immersion in SBF was nearly half (15.11%) of that observed for TiO_2–HA coating (about 27.69%).
iii The TiO_2–HA–PCL hybrid coating provided adequate protection to the Mg alloy in the presence of SBF and consequently delayed its degradation.
iv The Ca/P ratio of apatite deposited on TiO_2–HA–PCL hybrid coating suggested its bioactivity, bone growth and corrosion resistance better than TiO_2–HA coating.

Declaration of Competing Interest

The authors declare that they have no conflict of interest.

Acknowledgment

This work is funded under the research grant (File no. EMR/2016/001581) sponsored by SERB, DST, India.

References

[1] Y. Chen, Z. Xu, C. Smith, J. Sankar, Acta Biomater. (2014), doi:10.1016/j.actbio.2014.07.005.
[2] F. Witte, N. Hort, C. Vogt, S. Cohen, K. Ulrich, R. Willumeit, F. Feyerabend, Curr. Opin. Solid State Mater. Sci. 12 (2008) 63–72, doi:10.1016/j.cossms.2009.04.001.
[3] A. Yamamoto, S. Hiromoto, Mater. Sci. Eng. C 29 (2009) 1559–1568, doi:10.1016/j.msec.2008.12.015.
[4] J. Song, J. She, D. Chen, F. Pan, J. Magnes. Alloy 8 (2020) 1–41, doi:10.1016/j.jma.2020.02.003.
[5] T. Xu, Y. Yang, X. Peng, J. Song, F. Pan, J. Magnes. Alloy 7 (2019) 536–544, doi:10.1016/j.jma.2019.08.001.
[6] Z.Z. Yin, W.C. Qi, R.C. Zeng, X.B. Chen, C.D. Gu, S.K. Guan, Y.F. Zheng, J. Magnes. Alloy (2020), doi:10.1016/j.jma.2019.09.008.
[7] S. Yan, G. Song, S. Surfaces, Design of Tailored Biodegradable Implants: The Effect of Voltage on Electrodeposited CaP Coatings on Pure Magnesium, (n.d.) 0–3. https://doi.org/10.1111/jace.15888.
[8] R. Horváthová, L. Müller, P. Greil, F.A. Müller, In Vitro Transformation of OCP into Carbonated HA Under Physiological Conditions, 28 (2008) 1414–1419. https://doi.org/10.1016/j.msec.2008.03.010.
[9] P.I.I. Dissolution, Plasma Spraying of Zirconia-Reinforced Hydroxyapatite Composite Coatings on Titanium Part II Dissolution Behaviour in Simulated Body Fluid and Bonding Degradation, 8 (1997) 201–211.
[10] R. Azari, H.R. Rezaie, A. Khavandi, Investigation of Functionally Graded HA-TiO_2 Coating on Ti–6Al–4V Substrate Fabricated by Sol-Gel Method, Techna Group S.r.l., 2019, doi:10.1016/j.ceramint.2019.05.317.
[11] T. He, X. Guo, K. Zhang, Y. Feng, X. Wang, RSC Adv. 4 (2014) 5880–5886, doi:10.1039/c3ra44046j.
[12] H. Kim, H. Kim, V. Salih, J.C. Knowles, Hydroxyapatite and Titania Sol–Gel Composite Coatings on Titanium for Hard Tissue Implants; Mechanical and In Vitro Biological Performance, (2004) 1–8. https://doi.org/10.1002/jbm.b.30073.
[13] H. Tang, T. Xin, F. Wang, Calcium Phosphate/Titania Sol-Gel Coatings on AZ31 Magnesium Alloy for Biomedical Applications, 8 (2013) 8115–8125.
[14] P. Amaravathy, S. Sathyanarayanan, S. Sowndarya, N. Rajendran, Ceram. Int. 40 (2014) 6617–6630, doi:10.1016/j.ceramint.2013.11.119.
[15] S. Agarwal, J. Curtin, B. Duffy, S. Jaiswal, Mater. Sci. Eng. C 68 (2016) 948–963, doi:10.1016/j.msec.2016.06.020.
[16] R.N. Oosterbeek, C.K. Seal, M.P. Staiger, M.M. Hyland, J. Biomed. Mater. Res. – Part A 103 (2015) 311–317, doi:10.1002/jbm.a.35175.
[17] A. Zomorodian, C. Santos, M.J. Carmezim, T.M.E. Silva, J.C.S. Fernandes, M.F. Montemor, Electrochim. Acta 179 (2015) 431–440, doi:10.1016/j.electacta.2015.04.013.
[18] S. De Koker, B.G. De Geest, C. Cuvelier, L. Ferdinande, W. Deckers, W.E. Hennink, S. De Smedt, N. Mertens, Adv. Funct. Mater. 17 (2007) 3754–3763, doi:10.1002/adfm.200700416.
[19] L.Y. Li, L.Y. Cui, R.C. Zeng, S.Q. Li, X.B. Chen, Y. Zheng, M.B. Kannan, Acta Biomater. 79 (2018) 23–36, doi:10.1016/j.actbio.2018.08.030.
[20] S.R. Chastain, A.K. Kundu, S. Dhar, J.W. Calvert, A.J. Putnam, Adhesion of Mesenchymal Stem Cells to Polymer Scaffolds Occurs Via Distinct ECM Ligands and Controls their Osteogenic Differentiation, (2006). https://doi.org/10.1002/jbm.a.
[21] X. Xin, M. Hussain, J.J.M. Ã, Continuing Differentiation of Human Mesenchymal Stem Cells and Induced Chondrogenic and Osteogenic Lineages in Electrospun PLGA Nanofiber Scaffold, 28 (2007) 316–325. https://doi.org/10.1016/j.biomaterials.2006.08.042.
[22] A. Rezaei, M.R. Mohammadi, Mater. Sci. Eng. C 33 (2013) 390–396, doi:10.1016/j.msec.2012.09.004.
[23] L. Shor, Fabrication of Three-Dimensional Polycaprolactone/Hydroxyapatite Tissue Scaffolds and Osteoblast-Scaffold Interactions In Vitro, 28 (2007) 5291–5297. https://doi.org/10.1016/j.biomaterials.2007.08.018.
[24] J. Southgate, N.R. Cameron, S.C. Baker, Biomaterials the Relationship Between the Mechanical Properties and Cell Behaviour on PLGA and PCL Scaffolds for Bladder Tissue Engineering, 30 (2009) 1321–1328. https://doi.org/10.1016/j.biomaterials.2008.11.033.

[25] C.M. Agrawal, R.B. Ray, Biodegradable Polymeric Scaffolds for Musculoskeletal Tissue Engineering, (2000).
[26] E. Malikmammadov, T.E. Tanir, A. Kiziltay, V. Hasirci, N. Hasirci, PCL and PCL-based Materials in Biomedical Applications, Taylor & Francis, 2018, doi:10.1080/09205063.2017.1394711.
[27] H.M. Wong, Y. Zhao, F.K.L. Leung, T. Xi, Z. Zhang, Y. Zheng, S. Wu, K.D.K. Luk, K.M.C. Cheung, P.K. Chu, K.W.K. Yeung, Adv. Healthc. Mater. 6 (2017) 1–13, doi:10.1002/adhm.201601269.
[28] H.R. Bakhsheshi-Rad, E. Hamzah, M. Kasiri-Asgarani, S. Jabbarzare, N. Iqbal, M.R. Abdul Kadir, Mater. Sci. Eng. C 60 (2016) 526–537, doi:10.1016/j.msec.2015.11.057.
[29] Y. Chen, S. Zhao, M. Chen, W. Zhang, J. Mao, Y. Zhao, M.F. Maitz, N. Huang, G. Wan, Corros. Sci. 96 (2015) 67–73, doi:10.1016/j.corsci.2015.03.020.
[30] A. Abdal-Hay, K.C. In, J.K. Lim, Solid State Sci. 18 (2013) 131–140, doi:10.1016/j.solidstatesciences.2012.11.017.
[31] X. Li, X. Liu, S. Wu, K.W.K.K. Yeung, Y. Zheng, P.K. Chu, Acta Biomater. 45 (2016) 2–30, doi:10.1016/j.actbio.2016.09.005.
[32] B. Denkena, A. Lucas, F. Thorey, H. Waizy, N. Angrisani, A. Meyer-Lindenberg, Spec. Issues Magnes. Alloy (2011), doi:10.5772/22793.
[33] J. Stráský, J. Havlíková, L. Bačáková, P. Harcuba, M. Mhaede, M. Janeček, Appl. Surf. Sci. 281 (2013) 73–78, doi:10.1016/j.apsusc.2013.02.053.
[34] S. Mori, F.R. Lamastra, S. Kaciulis, P. Soltani, G. Montesperelli, Corros. Eng. Sci. Technol. 53 (2018) 44–53, doi:10.1080/1478422X.2017.1376943.
[35] U. Batra, S. Kapoor, S. Sharma, Influence of Magnesium Ion Substitution on Structural and Thermal Behavior of Nanodimensional Hydroxyapatite, 22 (2013) 1798–1806. https://doi.org/10.1007/s11665-012-0462-2.
[36] E. Tamjid, R. Bagheri, M. Vossoughi, A. Simchi, Mater. Lett. 65 (2011) 2530–2533, doi:10.1016/j.matlet.2011.05.037.
[37] M.M. Structure, H. Mechanical, J. Kim, K. Shin, Y. Koh, M.J. Hah, J. Moon, H. Kim, Production of Poly(ε -Caprolactone)/Hydroxyapatite Composite Scaffolds with a Tailored Macro/Micro-Porous Structure, High Mechanical Properties, and Excellent Bioactivity, (n.d.). https://doi.org/10.3390/ma10101123.
[38] G.R. Guillen, Y. Pan, M. Li, E.M.V Hoek, Preparation and Characterization of Membranes Formed by Nonsolvent Induced Phase Separation: A Review, (2011) 3798–3817.
[39] C. Yen, H. He, L.J. Lee, W.S.W. Ho, Synthesis and Characterization of Nanoporous Polycaprolactone Membranes Via Thermally- and Nonsolvent-Induced Phase Separations for Biomedical Device Application, 343 (2009) 180–188. https://doi.org/10.1016/j.memsci.2009.07.024.
[40] R. Azari, H.R. Rezaie, A. Khavandi, Ceram. Int. 45 (2019) 17545–17555, doi:10.1016/j.ceramint.2019.05.317.
[41] T.K. Ã, H. Takadama, How Useful is SBF in Predicting in Vivo Bone Bioactivity? $, 27 (2006) 2907–2915. https://doi.org/10.1016/j.biomaterials.2006.01.017.
[42] W. Jin, G. Wang, Z. Lin, H. Feng, W. Li, X. Peng, A.M. Qasim, P.K. Chu, Eval. Program Plann. (2016), doi:10.1016/j.corsci.2016.10.021.
[43] N.N. Aung, W. Zhou, Corros. Sci. 52 (2010) 589–594, doi:10.1016/j.corsci.2009.10.018.
[44] A.P. Md Saad, N. Jasmawati, M.N. Harun, M.R. Abdul Kadir, H. Nur, H. Hermawan, A. Syahrom, Corros. Sci. 112 (2016) 495–506, doi:10.1016/j.corsci.2016.08.017.
[45] D. Velten, V. Biehl, F. Aubertin, B. Valeske, W. Possart, J. Breme, Preparation of TiO2 Layers on cp-Ti and Ti6Al4V by Thermal and Anodic Oxidation and by Sol-Gel Coating Techniques and Their Characterization, (2001).
[46] N. Dumelie, H. Benhayoune, D. Richard, D. Laurent-maquin, G. Balossier, In Vitro Precipitation of Electrodeposited Calcium-Deficient Hydroxyapatite Coatings on Ti6Al4V Substrate, 59 (2006) 6–10. https://doi.org/10.1016/j.matchar.2006.11.030.
[47] A.M. Sofronia, R. Baies, E.M. Anghel, C.A. Marinescu, S. Tanasescu, Mater. Sci. Eng. C 43 (2014) 153–163, doi:10.1016/j.msec.2014.07.023.
[48] R.T. Selvi, A.P.S. Prasanna, R. Niranjan, M. Kaushik, T. Devasena, J. Kumar, R. Chelliah, D. Oh, S. Swaminathan, G.D. Venkatasubbu, Appl. Surf. Sci. (2018) 1–7, doi:10.1016/j.apsusc.2018.01.143.
[49] J. Krzaczkowska, Z. Fojud, M. Kozak, S. Jurga, Spectroscopic Studies of Poly (ε -Caprolactone)/ Sodium Montmorillonite Nanocomposites, 108 (2005) 187–196.
[50] M. Catauro, F. Papale, F. Bollino, J. Non. Cryst. Solids 415 (2015) 9–15, doi:10.1016/j.jnoncrysol.2014.12.008.
[51] P. Bhanuprakash, N.V.V Jyothi, C. Narasimharao, M. Raveendra, K. Sivakumar, C.R. PT, J. Mol. Liq. (2017), doi:10.1016/j.molliq.2017.03.056.
[52] M. Catauro, F. Bollino, R. Giovanardi, P. Veronesi, Mater. Sci. Eng. C (2016), doi:10.1016/j.msec.2016.12.046.
[53] M. Ravi, S. Song, J. Wang, Ionics (2016) 661–670, doi:10.1007/s11581-015-1586-9.
[54] L. Xu, A. Yamamoto, Colloids Surf. B Biointerfaces 93 (2012) 67–74, doi:10.1016/j.colsurfb.2011.12.009.
[55] E. Hamzah, S.N. Saud, J. Mater. Eng. Perform. 24 (2015) 4010–4021, doi:10.1007/s11665-015-1661-4.
[56] S.Z. Fu, X.H. Wang, G. Guo, S. Shi, M. Fan, H. Liang, F. Luo, Z.Y. Qian, J. Biomed. Mater. Res. – Part B Appl. Biomater. 97 B (2011) 74–83, doi:10.1002/jbm.b.31788.
[57] L. Cui, P. Qin, X. Huang, Z. Yin, R. Zeng, S. Li, Surf. Coat. Technol. 324 (2017) 560–568, doi:10.1016/j.surfcoat.2017.06.015.
[58] M. Jamesh, S. Kumar, T.S.N. Sankara Narayanan, T.S.N.S. Narayanan, Corros. Sci. 53 (2011) 645–654, doi:10.1016/j.corsci.2010.10.011.
[59] A. Conde, A. Durán, J.J. De Damborenea, Polymeric Sol–Gel Coatings as Protective Layers of Aluminium Alloys, 46 (2003) 288–296. https://doi.org/10.1016/S0300-9440(03)00014-6.
[60] Z.G. Huan, M.A. Leeflang, J. Zhou, L.E. Fratila-Apachitei, J. Duszczyk, J. Mater. Sci. Mater. Med. 21 (2010) 2623–2635, doi:10.1007/s10856-010-4111-8.
[61] M.M. Monteiro, N. Carbonel, G.D.A. Soares, Dissolution Properties of Calcium Phosphate Granules with Different Compositions in Simulated Body Fluid, (2002) 1–7.
[62] W.L. Suchanek, K. Byrappa, P. Shuk, R.E. Riman, V.F. Janas, K.S. Tenhuisen, Biomaterials 25 (2004) 4647–4657, doi:10.1016/j.biomaterials.2003.12.008.
[63] N. Kanasan, S. Adzila, H.A. Rahman, N. Bano, G. Panerselvan, N.A. Hidayati, Key Eng. Mater. 791 (2018) 45–49, doi:10.4028/www.scientific.net/KEM.791.45.
[64] A. Farzadi, F. Bakhshi, M. Solati-Hashjin, M. Asadi-Eydivand, N.A.A. Osman, Ceram. Int. 40 (2014) 6021–6029, doi:10.1016/j.ceramint.2013.11.051.
[65] A. Witecka, A. Bogucka, A. Yamamoto, K. Máthis, T. Krajňák, J. Jaroszewicz, W. Święszkowski, Ś. Wojciech, Mater. Sci. Eng. C 65 (2016) 59–69, doi:10.1016/j.msec.2016.04.019.
[66] H. Tang, D. Yu, Y. Luo, F. Wang, Appl. Surf. Sci. 264 (2013) 816–822, doi:10.1016/j.apsusc.2012.10.146.
[67] H. Wang, S. Guan, Y. Wang, H. Liu, H. Wang, L. Wang, C. Ren, S. Zhu, K. Chen, Colloids Surf. B Biointerfaces 88 (2011) 254–259, doi:10.1016/j.colsurfb.2011.06.040.
[68] Y. Zhao, H. Liu, C. Li, Y. Chen, S. Li, Appl. Surf. Sci. 434 (2018) 787–795, doi:10.1016/j.apsusc.2017.11.012.
[69] I. Cacciotti, Cationic and Anionic Substitutions in Hydroxyapatite, n.d. https://doi.org/10.1007/978-3-319-12460-5.
[70] F. Ren, Y. Leng, R. Xin, X. Ge, Acta Biomater. 6 (2010) 2787–2796, doi:10.1016/j.actbio.2009.12.044.
[71] L. Mayer, R. Scblam, J.D.B. Featberstone, Magnesium-Containing Carbonate Apatite, (1997).
[72] D. Laurencin, N. Almora-barrios, N.H. De Leeuw, C. Gervais, C. Bonhomme, F. Mauri, W. Chrzanowski, J.C. Knowles, R.J. Newport, A. Wong, Z. Gan, M.E. Smith, Biomaterials 32 (2011) 1826–1837, doi:10.1016/j.biomaterials.2010.11.017.
[73] I. Johnson, J. Lin, H. Liu, Surface Modification and Coatings for Controlling the Degradation and Bioactivity of Magnesium Alloys for Medical Applications, 2017.

Please cite this article as: N. Singh, U. Batra, K. Kumar et al., Investigating TiO2–HA–PCL hybrid coating as an efficient corrosion resistant barrier of ZM21 Mg alloy, Journal of Magnesium and Alloys, https://doi.org/10.1016/j.jma.2020.08.003